Molecular Cell

Article

AMPK directly phosphorylates TBK1 to integrate glucose sensing into innate immunity

Graphical abstract

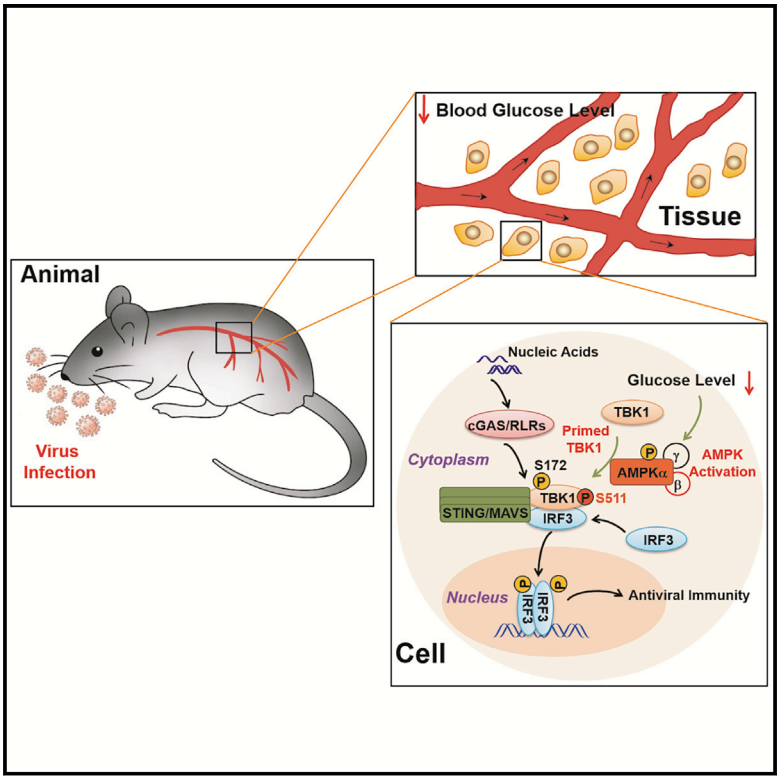

Highlights

- Viral infection induces acute blood glucose decline in rodents that activates AMPK
- AMPK directly phosphorylates TBK1 at S511 to prime antiviral sensing
- AMPK-TBK1 couples glucose deficiency sensing and innate immune surveillance
- Targeting the AMPK-TBK1 axis compromises innate antiviral immunity

Authors

Qian Zhang, Shengduo Liu, Chen-Song Zhang, ..., Xin-Hua Feng, Sheng-Cai Lin, Pinglong Xu

Correspondence

xupl@zju.edu.cn

In brief

The relevance between blood glucose levels and antiviral defense is long appreciated, but not its molecular basis. Zhang et al. identify an inherent function of the energy regulator AMPK, which couples glucose and nucleic acid dual sensing via an elegant AMPK-TBK1 cascade and connects physiological glucose levels to antiviral immunity.

Zhang et al., 2022, Molecular Cell *82*, 1–18
December 1, 2022
https://doi.org/10.1016/j.molcel.2022.10.026

CellPress

Molecular Cell

CellPress

Article

AMPK directly phosphorylates TBK1 to integrate glucose sensing into innate immunity

Qian Zhang,[1,2,3,11] Shengduo Liu,[1,2,11] Chen-Song Zhang,[4,11] Qirou Wu,[1] Xinyuan Yu,[1] Ruyuan Zhou,[1,2] Fansen Meng,[1] Ailian Wang,[1] Fei Zhang,[1,3] Shasha Chen,[1,5] Xiaojian Wang,[6] Lei Li,[1] Jun Huang,[1] Yao-Wei Huang,[7] Jian Zou,[8] Jun Qin,[9] Tingbo Liang,[3,10] Xin-Hua Feng,[1,10] Sheng-Cai Lin,[4] and Pinglong Xu[1,2,3,10,*]

[1]The MOE Key Laboratory of Biosystems Homeostasis & Protection and Zhejiang Provincial Key Laboratory of Cancer Molecular Cell Biology, Life Sciences Institute, Zhejiang University, Hangzhou 310058, Zhejiang, China

[2]Institute of Intelligent Medicine, Hangzhou Global Scientific and Technological Innovation Center, Zhejiang University (HIC-ZJU), Hangzhou 310058, China

[3]Department of Hepatobiliary and Pancreatic Surgery and Zhejiang Provincial Key Laboratory of Pancreatic Disease, The First Affiliated Hospital, University School of Medicine, Zhejiang University, Hangzhou 310058, China

[4]State Key Laboratory for Cellular Stress Biology, School of Life Sciences, Xiamen University, Xiamen 361102, China

[5]Zhejiang Provincial Key Laboratory for Water Environment and Marine Biological Resources Protection, College of Life and Environmental Science, Wenzhou University, Wenzhou 325035, China

[6]Institute of Immunology, Zhejiang University School of Medicine, Hangzhou 310058, China

[7]Key Laboratory of Animal Virology of Ministry of Agriculture, College of Animal Sciences, Zhejiang University, Hangzhou 310058, China

[8]Eye Center of the Second Affiliated Hospital School of Medicine, Institutes of Translational Medicine, Zhejiang University, Hangzhou 310058, China

[9]CAS Key Laboratory of Tissue Microenvironment and Tumor, Center for Excellence in Molecular Cell Science, Shanghai Institute of Nutrition and Health, Chinese Academy of Sciences, Shanghai 200031, China

[10]Cancer Center, Zhejiang University, Hangzhou 310058, Zhejiang, China

[11]These authors contributed equally

*Correspondence: xupl@zju.edu.cn

https://doi.org/10.1016/j.molcel.2022.10.026

SUMMARY

Nutrient sensing and damage sensing are two fundamental processes in living organisms. While hyperglycemia is frequently linked to diabetes-related vulnerability to microbial infection, how body glucose levels affect innate immune responses to microbial invasion is not fully understood. Here, we surprisingly found that viral infection led to a rapid and dramatic decrease in blood glucose levels in rodents, leading to robust AMPK activation. AMPK, once activated, directly phosphorylates TBK1 at S511, which triggers IRF3 recruitment and the assembly of MAVS or STING signalosomes. Consistently, ablation or inhibition of AMPK, knockin of TBK1-S511A, or increased glucose levels compromised nucleic acid sensing, while boosting AMPK-TBK1 cascade by AICAR or TBK1-S511E knockin improves antiviral immunity substantially in various animal models. Thus, we identify TBK1 as an AMPK substrate, reveal the molecular mechanism coupling a dual sensing of glucose and nuclei acids, and report its physiological necessity in antiviral defense.

INTRODUCTION

Responses to invasion and damage are fundamental processes in living organisms. Cytosolic nucleic acid sensors such as RIG-I[2] and cGAS[3,4] monitor invading microbes and damage by perceiving cytosolic nucleic acids derived from pathogens, the nucleus, or the mitochondria.[5–8] RNA sensors RIG-I and MDA5, activated by viral RNA species, interact with and promote mass aggregation of MAVS (known as VISA, IPS-1, or Cardif) on the mitochondrial surface to form the MAVS signalosome.[9,10] Second messenger 2′3′-cyclic GMP-AMP (cGAMP),[3,11–13] synthesized by DNA sensor cGAS, activates STING (also known as MITA or ERIS)[14–16] to trigger a non-canonical STING-PERK pathway initiated in the endoplasmic reticulum (ER) that regulates mRNA translation.[17] Subsequently, STING translocates to the ERGIC/Golgi apparatus, where the STING signalosome assembles, facilitated by TBK1 activation and the IRF3 recruitment.[18,19] IRF3 phosphorylation at the C terminus by TBK1 in the MAVS or STING signalosome mobilizes its dimerization and nuclear translocation, where IRF3 transcribes type I interferons (IFN-Is) and numerous IFN-stimulated genes (ISGs), directly and indirectly,[20,21] in coordination with simultaneously activated NF-κB.[5–7] Nucleic acid sensing establishes an immune state to restrict microbial infection, modulates adaptive immunity, and guides tissue repair and regeneration.[5–7,22,23]

Please cite this article in press as: Zhang et al., AMPK directly phosphorylates TBK1 to integrate glucose sensing into innate immunity, Molecular Cell (2022), https://doi.org/10.1016/j.molcel.2022.10.026

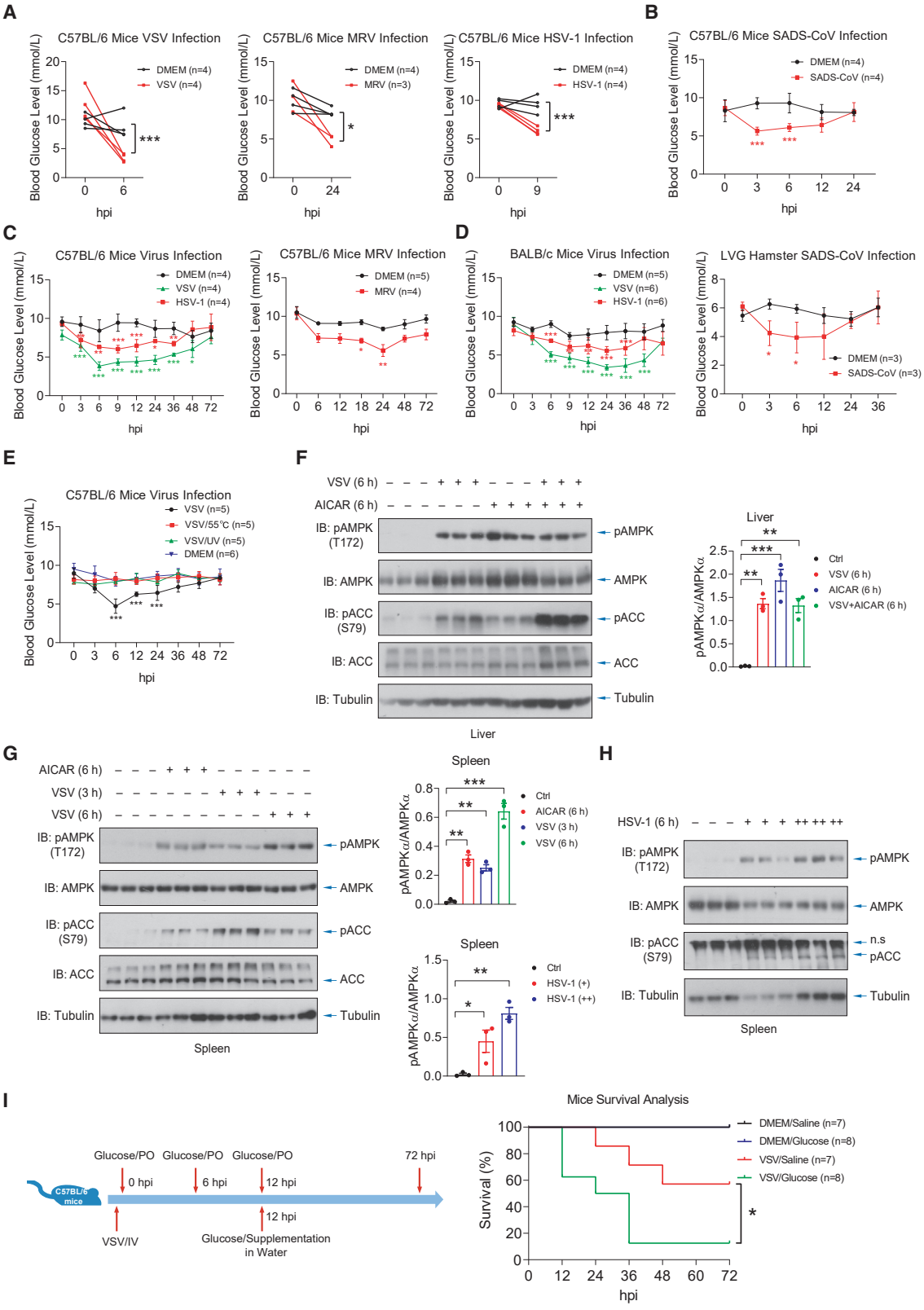

(legend on next page)

Please cite this article in press as: Zhang et al., AMPK directly phosphorylates TBK1 to integrate glucose sensing into innate immunity, Molecular Cell (2022), https://doi.org/10.1016/j.molcel.2022.10.026

At the cellular level, nucleic acid sensing controls autophagy,[24–26] senescence,[27–30] protein synthesis,[17] protein condensation,[31] mitochondrial dynamics,[10] and differentiation,[32] and triggers cell death.[33–35] TBK1, the central kinase in MAVS and STING signalosomes,[36] is activated by intermolecular *trans*-autophosphorylation[19,37] and regulated elaborately by host factors, microbial proteins, and environmental cues.[38–40] Known posttranslational modifiers of TBK1 include IKKβ,[41] LCK,[42] SRC,[43] AKT1,[44] PKCθ,[45] and DYRK2.[46] Nevertheless, the components and precise mechanisms related to STING and MAVS signalosomes' translocation, assembly, and activation are incomplete.

Metazoan cells also rely on the balanced availability of nutrients, including glucose and amino acids, to maintain proliferation and survival. However, a direct molecular link between two basic cellular behaviors, the sensing of nutrients and the perception of damage, has barely been established thus far. AMP-activated protein kinase (AMPK) is a principal sensor of glucose deficiency and the master controller of various metabolic pathways.[47–49] Notably, AMPK is activated at the lysosomal surface in response to decreasing glucose levels through aldolase and the v-ATPase-Ragulator complex,[50,51] besides being controlled by AMP/ATP ratios and crosstalk with other signaling pathways.[48,52,53] Once activated, AMPK impacts cell physiology, such as glucose and lipid metabolism, protein synthesis, autophagy and mitochondrial biogenesis, and whole-body metabolism.[48,54] The therapeutic potential of AMPK is broadly recognized in treating metabolic diseases such as obesity, type 2 diabetes, and cancer. AMPK restricts the replication of microbial pathogens, such as hepatitis C virus (HCV), Rift Valley Fever virus (RVFV), and *M. tuberculosis*,[55–57] although the underlying mechanism is largely undetermined. The pathogens also employ the strategy of AMPK inhibition to manipulate the innate host response.[57] Besides, AMPK functions in T cell metabolism by controlling T cell metabolic plasticity.[58] Intriguingly, a recent report indicates a critical function of TBK1 in adipocytes for repressing energy expenditure by direct phosphorylation and inhibition of AMPKα.[59] However, the role of AMPK in innate immunity has barely been explored, and neither its physiological significance nor its key molecular events are precisely determined.[59,60]

Hyperglycemia, the prominent metabolic feature in diabetes patients, has been considerably linked to diabetes-related vulnerability to microbial and parasitic infection. Infections are more frequent and severer in diabetic versus non-diabetic individuals, including increased occurrences and severities of lung infection by Influenza virus (IAV), *Legionella* spp., and *M. tuberculosis*, blood infection by Dengue virus (DENV), brain infection by West Nile virus (WNV),[61] liver infection by HCV, and skin lesion by Varicella-Zoster virus (VZV, Herpes Zoster).[62,63] Notably, diabetes and poor glycemic control are closely associated with the severity and mortality of patients with COVID-19[64–66] and severe acute respiratory syndrome (SARS).[67] Thus, we systemically investigate the connection between glucose sensing and nucleic acid sensing. Unexpectedly, we found that AMPK is robustly activated in various tissues during the very early stage of viral infection due to a rapid and sharp drop in blood glucose levels. AMPK then directly phosphorylates TBK1 at S511 to prime the assembly of STING and MAVS signalosomes, thus potentiating pathogen and damage surveillance. The genetic or pharmacologic intervention of this AMPK-directed TBK1 modification severely impedes innate immune sensing and antiviral immunity. Together, we describe an intrinsic and essential function of AMPK for coupling glucose and damage sensing.

RESULTS

Viral infection induces a rapid and dramatic drop in blood glucose levels

To survey the physiological interplay between glucose sensing and danger recognition, we constantly monitored the blood glucose levels of mice (C57BL/6) infected with RNA and DNA viruses. Unexpectedly, we detected striking decreases in murine serum glucose levels upon infection of vesicular stomatitis virus (VSV), mammalian orthoreovirus (MRV), HSV-1 (Figure 1A), and swine acute diarrhea syndrome coronavirus (SADS-CoV) (Figure 1B). The degree of blood glucose drop was remarkable; blood glucose was considered extremely low (3.5–5 mM/L, roughly 60–90 mg/dL) (Figures 1A–1C). Similar alterations were seen in viral-infected BALB/c mice and LVG hamsters (Figure 1D). They occurred rapidly, peaked at 6–24 h post-infection (hpi) depending on the mouse strain/virus type, and were resolved by 36–48 hpi (Figures 1B–1D), even in mice without food supplements (Figure S1A) or with per os (P.O.) gavage of foods (Figure S1B). However, the infected mice consumed less food at 48 hpi (Figure S1C). Intriguingly, viral inactivation by either thermal treatment or UV exposure eliminated the decline of glucose levels (Figure 1E), suggesting that viral nucleic acids-carried information instead of humoral immunity causes

Figure 1. Viral infection results in rapid and dramatic decreases in blood glucose levels and AMPK activation

(A) The glucose levels in the serum of C57BL/6 mice were surveyed at the indicated time upon intravenous infection with VSV or HSV-1 by tail injection or intragastric MRV infection.

(B and C) The blood glucose levels of C57BL/6 mice were constantly monitored upon viral infection.

(D) Infection of RNA virus VSV, coronavirus SADS-CoV, or DNA virus HSV-1 reduced blood glucose levels in BALB/c mice or LVG hamsters.

(E) Inactivated by thermal exposure (55°C, 1 h) or UV exposure (8,000 J/m^2, 20 min), VSV failed to reduce blood glucose levels.

(F–H) Activation of endogenous AMPK in organs was indicated by phospho-AMPK T172 and phospho-ACC immunoblottings in response to VSV infection (F and G), AICAR treatment (5 mg/kg, 6 h) (F and G), or HSV-1 infection (6 h) (H).

(I) C57BL/6 mice were challenged with VSV via tail injection, without or with per os (P.O.) gavage administration of glucose and afterward 20% glucose supplementation in drinking water, and the survival ratio was monitored at desired stages. The number of mice used is indicated. * $p = 0.0401$, by log-rank test. Applied to Figures 1, 2, 3, 4, 5, 6, and 7: unless specified, n = 3 independent experiments (mean ± SEM); * $p < 0.05$, ** $p < 0.01$, and *** $p < 0.001$, by statistical analysis of the indicated comparison with ANOVA and Bonferroni correction; unprocessed images are shown in Mendeley Data.

See also Figure S1.

Please cite this article in press as: Zhang et al., AMPK directly phosphorylates TBK1 to integrate glucose sensing into innate immunity, Molecular Cell (2022), https://doi.org/10.1016/j.molcel.2022.10.026

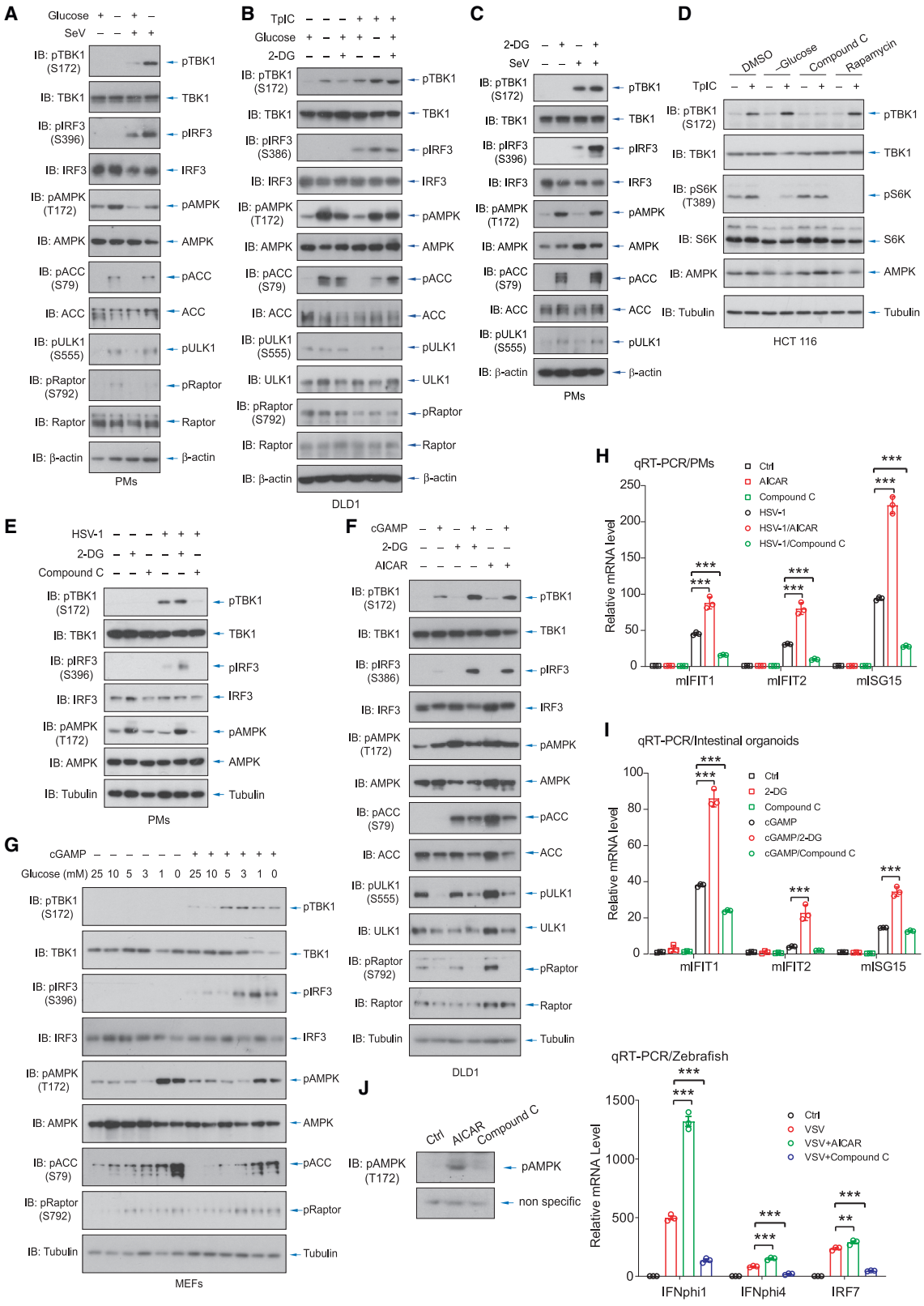

(legend on next page)

Please cite this article in press as: Zhang et al., AMPK directly phosphorylates TBK1 to integrate glucose sensing into innate immunity, Molecular Cell (2022), https://doi.org/10.1016/j.molcel.2022.10.026

this dramatic effect. The process might be relevant to innate immune responses, such as those mediated by TBK1-activated glycolysis in cells[68,69] or the TLR-CNS axis,[70] but waiting to be determined.

The rapid and sharp drop in blood glucose levels activates AMPK in tissues

Reductions in blood glucose levels will intrinsically lead to AMPK activation due to the ancestral role of AMPK in glucose sensing.[49] We found that AMPK was remarkably and rapidly activated in the livers and spleens of mice with infection of RNA virus VSV (Figures 1F and 1G) or DNA virus HSV-1 (Figure 1H) to a level comparable to the treatment of AICAR, a highly selective and potent activator of AMPK.[71] As also evidenced by the phosphorylation of AMPK substrates, AMPK activation was evident and preceded TBK1-IRF3 activation (Figures S1D). The AMPKAR-EV transgenic mice[72] were employed to monitor the real-time AMPK activity of skeletal muscle via *in vivo* imaging. In the biceps femoris, fluorescence resonance energy transfer (FRET)/cyan fluorescent protein (CFP) ratios revealed that VSV infection triggered a marked activation of endogenous AMPK similar to AICAR treatment (Figure S1E). Additionally, the VSV-challenged mice had a faster progression and more severity of the infectious disease when the drop in blood glucose was partially compromised (maintain roughly 6–10 mM/L) by oral gavage or drinking water supplement of glucose (Figure 1I). These observations indicate the physiological importance of this sharp drop in glucose blood levels.

What causes this dramatic *in vivo* activation of AMPK? We employed a CE-MS methodology that revealed the barely affected AMP/ADP:ATP ratios in the peritoneal macrophages (PMs) at a time scale (2–3 hpi) with dramatic AMPK activation (Figures S1D, S1F, and S1G), suggesting that the sharp drop in blood glucose levels triggers AMPK activation, rather than energy deficiency in cells replicating viruses. Additionally, VSV infection did not dramatically disturb long-chain fatty acids metabolism and enhanced circulating free fatty acids (FAAs) at the early stage of infection (Figure S1H), favoring that this AMPK activation is independent of long-chain fatty acid (LCFA) metabolism.[73]

Glucose deficiency magnifies nucleic acid sensing via AMPK

Innate immune responses were then examined in innate immune cells (PMs), epithelial cells (DLD1 and HCT 116), and fibroblasts (MEFs). Infection with RNA virus SeV activated TBK1 and IRF3 in PMs, which was substantially boosted by glucose starvation that activated AMPK (Figure 2A). We instead transfected poly(I:C) (TpIC), a dsRNA analog, to exclude the possible involvement of virally encoded proteins. Poly(I:C) similarly caused striking TBK1 and IRF3 activation under glucose-deficient conditions (Figure 2B). Similarly, SeV-induced TBK1 activation in PMs and MEFs was potentiated by 2-DG treatment that activated AMPK (Figures 2C and S2A). Sensing of mtDNAs, released upon the treatment of ABT-737, qVD-OPH, and S63845 (AQS), was similarly augmented by glucose depletion (Figure S2B).

Two critical regulators of cellular energy metabolism, the AMPK and mTOR, were examined to understand glucose deficiency-enhanced nucleic acid sensing. Inhibition of AMPK by Compound C, but not the blockade of mTOR by rapamycin, prevented TBK1 activation (Figure 2D), and AMPK inhibition attenuated both RNA and DNA sensing (Figures 2E and S2C). We then evaluated AICAR and A-769662,[74] two well-defined AMPK agonists that function through distinct mechanisms. cGAMP-induced STING-TBK1-IRF3 signaling was profoundly enhanced by AICAR, A-769662, or 2-DG (Figures 2F and S2D). Notably, we revealed the substantially potentiated STING-TBK1-IRF3 signaling in MEFs, near *in vivo* blood glucose levels in infected rodents (<5 mM) (Figure 2G). These findings suggest a physiological connection between blood glucose drop, AMPK activation, and enhanced nucleic acid sensing.

Nucleic acid sensing-initiated cytokine expression in tissues requires AMPK activity

We next examined mRNAs of IFN-Is and ISGs in macrophages, intestinal organoids, and zebrafish to characterize the dual sensing of glucose and nucleic acids. AMPK agonist AICAR robustly potentiated, but inhibitor Compound C profoundly attenuated the HSV-1-induced ISGs mRNAs in PMs (Figure 2H). We found that intestinal organoids cultured *in vitro* were sensitive and functioned as convenient tissue models for nucleic acid sensing study. cGAS-STING signaling in intestinal organoids stimulated by hydroxyurea (HU) or cGAMP was markedly enhanced by AICAR or 2-DG but suppressed by Compound C (Figures 2I and S2E). Zebrafish is an ideal model for evaluating innate immune responses.[40,75,76] VSV infection in zebrafish triggered robust antiviral responses via induction of zIFNφs and zISGs, and AICAR was able to activate zebrafish AMPK (zAMPK) (Figure 2J, left) and augmented antiviral responses (Figure 2J,

Figure 2. Glucose deficiency facilitates nucleic acid sensing via AMPK

(A–C) Cytosolic RNA sensing was evaluated in PMs under glucose starvation and 2-DG administration in response to SeV infection (A and C) or cytosolic exposure of RNA analogs poly(I:C) (B), as indicated by immunoblotting using antibodies recognizing active forms of TBK1 and IRF3.

(D) Glucose deficiency potentiated RNA sensing, which was attenuated by AMPK inhibitor Compound C but not mTOR inhibitor rapamycin.

(E) The effects of 2-DG administration and Compound C on DNA sensing were evaluated in PMs infected with HSV-1.

(F and G) AMPK activation by 2-DG, AICAR, or low glucose concentration promoted cGAS-STING signaling in DLD1 cells (F) and MEFs (G), stimulated by STING agonist cGAMP.

(H) The effects of AICAR and Compound C on DNA sensing were evaluated in PMs infected with HSV-1 by the mRNA expression of ISGs.

(I) Intestinal organoids from crypts isolated from mouse intestines were cultured *in vitro* and stimulated by cGAMP to activate DNA sensing. Effects of 2-DG and Compound C on DNA sensing were evaluated by ISGs expression. n = over 600 organoids from 3 mice in each group.

(J) gVSV was microinjected into the yolks of zebrafish embryos to elicit a robust viral infection state. Zebrafish embryos at 24 hpi were subjected to immunoblotting and qRT-PCR analysis to determine the effects of AICAR or Compound C on zebrafish AMPK activation (J, left) and mRNA expression of zebrafish IFNs and ISGs (J, right), respectively. n = 3 independent experiments using 25 embryos in each group.

See also Figure S2.

Please cite this article in press as: Zhang et al., AMPK directly phosphorylates TBK1 to integrate glucose sensing into innate immunity, Molecular Cell (2022), https://doi.org/10.1016/j.molcel.2022.10.026

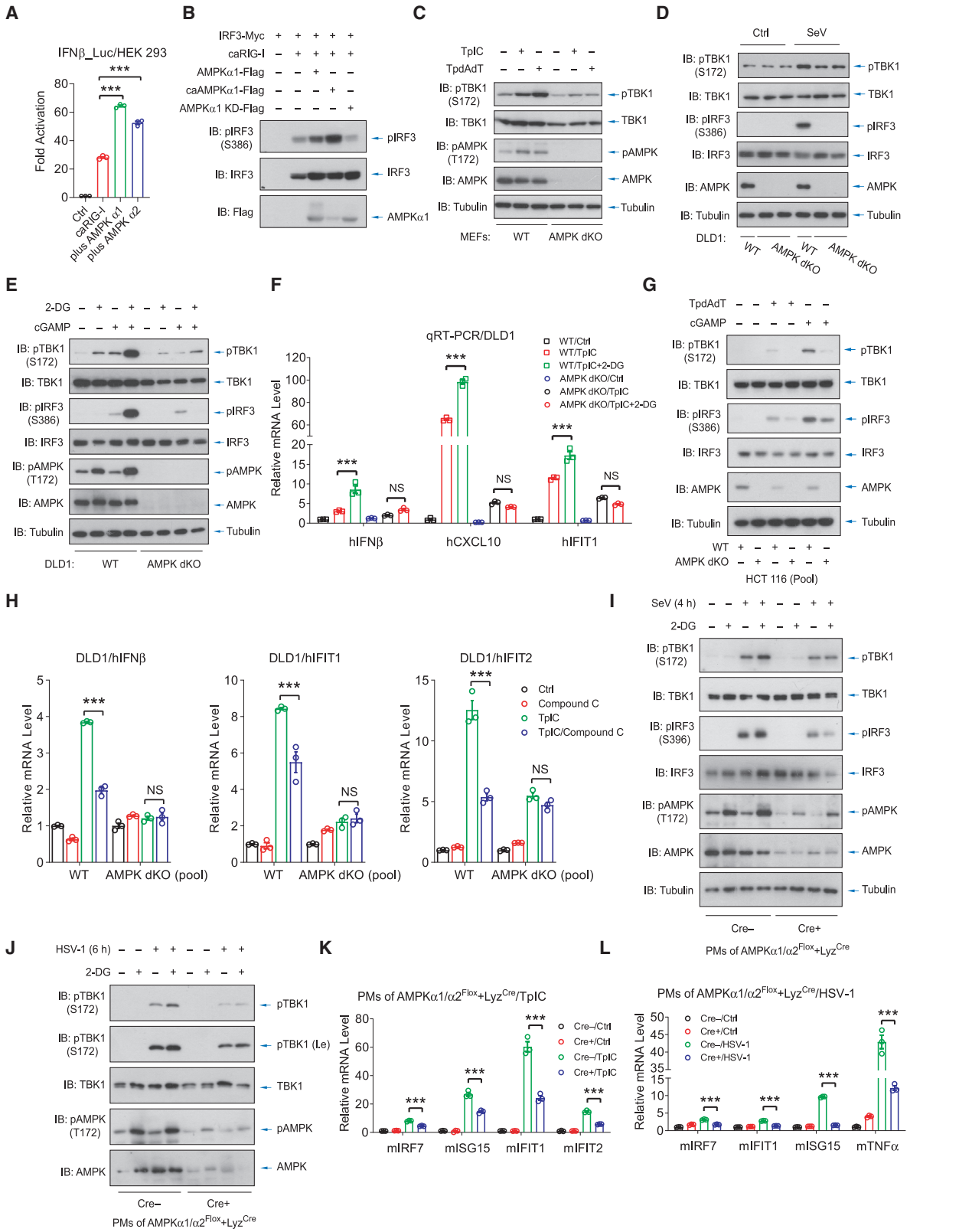

(legend on next page)

Please cite this article in press as: Zhang et al., AMPK directly phosphorylates TBK1 to integrate glucose sensing into innate immunity, Molecular Cell (2022), https://doi.org/10.1016/j.molcel.2022.10.026

right). These collective observations suggest that AMPK activity is a crucial and cross-species physiological determinant for cytokine production upon nucleic acid sensing.

Genetic ablation of AMPK attenuates nucleic acid sensing

Via cotransfection, we found that expression of AMPKα (catalytic) subunits strongly promoted RIG-I- or TBK1-stimulated IRF3 transactivation (Figures 3A and S3A), relying on the AMPK kinase activity in a dose-dependent manner (Figures 3B and S3B). Next, various AMPK genetic tools were then employed to validate the role of AMPK in innate immunity. MEFs from mice with genetic ablation of both AMPKα subunits (dKO) reduced dsDNA sensing (Figure 3C) and dsRNA sensing (Figures 3C and 3D). CRISPR-mediated dKO of AMPK α1/α2 subunits in DLD1 cells led to compromised SeV sensing (Figure 3D), damage-induced DNA sensing (Figure S3E), and STING signaling (Figure 3E). Without AMPKα subunits, 2-DG failed to enhance STING signaling (Figure 3E) and RNA sensing-induced IFN-Is and ISGs expression (Figure 3F). These data suggest an essential role of AMPK in the effective sensing of cytosolic RNAs and DNAs.

We also generated a gRNA-transfected pool of HCT116 and DLD1 cells to exclude the interference of distinct clonal backgrounds and inspect this effect. AMPK deletion/depletion by gRNAs attenuated cGAS-STING signaling (Figure 3G) and RNA sensing-induced expression of IFN-Is and ISGs (Figure S3F), as well as the inhibitory effect of Compound C (Figure 3H). Besides, PMs obtained from the mice with conditional knockout of AMPKα1/α2 in a myeloid line (AMPKα1/α2^{Flox}+Lyz^{Cre}) showed the strongly compromised sensing of SeV and HSV-1 (Figures 3I and 3J), and attenuated mRNA expression of IFN-Is and ISGs (Figures 3K and 3L). These observations suggest that AMPK is physiologically vital for effectively sensing cytosolic nucleic acids.

TBK1 is a substrate of AMPK modified at a classic substrate motif

We then attempted to decipher the molecular mechanism underlying the AMPK-potentiated nucleic acid sensing. Coimmunoprecipitation revealed an interaction between cotransfected TBK1 and the AMPK α and β subunits (Figure 4A) and a complex of stably expressed AMPKα with endogenous TBK1 and IRF3 in MEFs and gut epithelial cells (Figures 4B, S4A, and S4B), particularly upon AMPK activation. Domain mapping analysis using AMPKα1 truncation mutants revealed that the N terminus kinase domain of AMPKα1 was responsible and sufficient for TBK1 interaction (Figure 4C). These data suggest a stimulating interaction between AMPK and TBK1.

An interaction of TBK1 with the kinase domain of AMPK implies a potentially direct modification of TBK1 by AMPK. Intriguingly, we observed a somewhat AMPK-mediated mobility shift signal for TBK1 in Phos-tag electrophoresis (Figure 4D), a clue of AMPK-mediated TBK1 phosphorylation. Scansite software (https://scansite4.mit.edu) predicts that the S511 and T682 residues of TBK1 are possibly modified by AMPK. Notably, the amino acid sequence proximal to S511 has perfectly matched the classic AMPK recognition motif, featuring the hydrophobic residues at −5 (L) and +4 (I) and a basic residue at −3 or −4 (R) (Figure 4E), both of which are important for substrate recognition.[77] In addition, TBK1 S511 residue has a polar side chain at +3 (T) and a neutral polar residue at −2 (S) (Figure 4E), which further enhances AMPK modification.[78,79] This well-matched AMPK substrate motif on TBK1 is highly conserved among vertebrates (Figure S4C). Notably, mass spectrometry analysis for coexpressed TBK1 and AMPK revealed that S511, but not T682, was phosphorylated by AMPKα1. This phosphorylation was entirely prevented by Compound C (Figure S4D). We then collaborated with Abcam to generate an antibody explicitly targeting the phospho-TBK1 S511 due to the unavailability of a commercial antibody recognizing the AMPK substrate motif with a basic residue at the −4 position. The resulting antibody recognized the specific TBK1 phospho-S511 residue but did not cross-react with the proximal phospho-S510 targeted by AKT1[44] (Figure 4F), while mutating the S511 residue into alanine eliminated this phosphorylation signal (Figure 4G). Besides, phospho-TBK1 S511 was not induced by AKT1 but augmented upon the suppression of AKT activity, as revealed by mass spectrometry assay (Figure S4E). To exclude the possibility of an AMPK-ULK-mediated modification at TBK1 S511, we generated L508R mutant TBK1 by which a putative ULK1 substrate motif is disrupted and R507A mutant that disrupts the AMPK substrate motif. Evidently, disruption of the AMPK motif eliminated the phosphorylation signal while mutating the putative ULK1/2 motif not, suggesting AMPKα1 phosphorylates TBK1 directly at S511 (Figure 4H). Notably, VSV infection or AICAR treatment potentiated endogenous AMPK and phospho-TBK1 S511 in murine livers or spleens (Figures 4I and S4F) and DLD1 cells (Figure S4G), with an observable activation flow through AMPK, pTBK1 S511, pTBK1 S172, and pIRF3 (Figure 4I). Meanwhile, deletion/depletion of AMPKα1/α2, but not ULK1/2 or FIP200, an essential partner of ULK1/2, abrogated endogenous TBK1

Figure 3. Genetic ablation of AMPK attenuates nucleic acid sensing

(A and B) The effects of AMPKα1 or α2 in RIG-I-N (caRIG-I)-stimulated IRF3 transactivation was assessed by IRF3-responsive reporter assay (A) and phospho-IRF3 immunoblotting (B).

(C) AMPKα1/α2 dKO MEFs were insensitive to sensing of RNA or DNA analogs, evidenced by attenuated TBK1 activation.

(D and E) AMPKα1/α2 dKO DLD1 cells were generated by CRISPR-mediated genome editing, verified by immunoblotting, and analyzed the sensing of cytosolic RNA (D) and cGAMP-induced STING signaling (E).

(F) The dKO of AMPK α subunits reduced TpIC-stimulated RNA sensing and abolished the effects of 2-DG on RNA sensing-initiated expression of IFNβ and ISGs.

(G and H) Cell pools of HCT116 and DLD1 with deficiency of AMPKα1/α2 were generated by gRNA-mediated strategy and analyzed for TBK1 and IRF3 activation (G) and the mRNA expression of IFN-β and ISGs (H). dKO of AMPK eliminated the difference caused by Compound C treatment (H).

(I and J) In PMs obtained from AMPKα1/α2 conditional dKO mice, the enhanced sensing of the SeV (I) and HSV-1 (J) by 2-DG administration was lost.

(K and L) Genetic ablation of AMPKα1/α2 in PMs resulted in profound decreases in ISG mRNA expression upon RNA sensing (K) or DNA sensing (L).

See also Figure S3.

Please cite this article in press as: Zhang et al., AMPK directly phosphorylates TBK1 to integrate glucose sensing into innate immunity, Molecular Cell (2022), https://doi.org/10.1016/j.molcel.2022.10.026

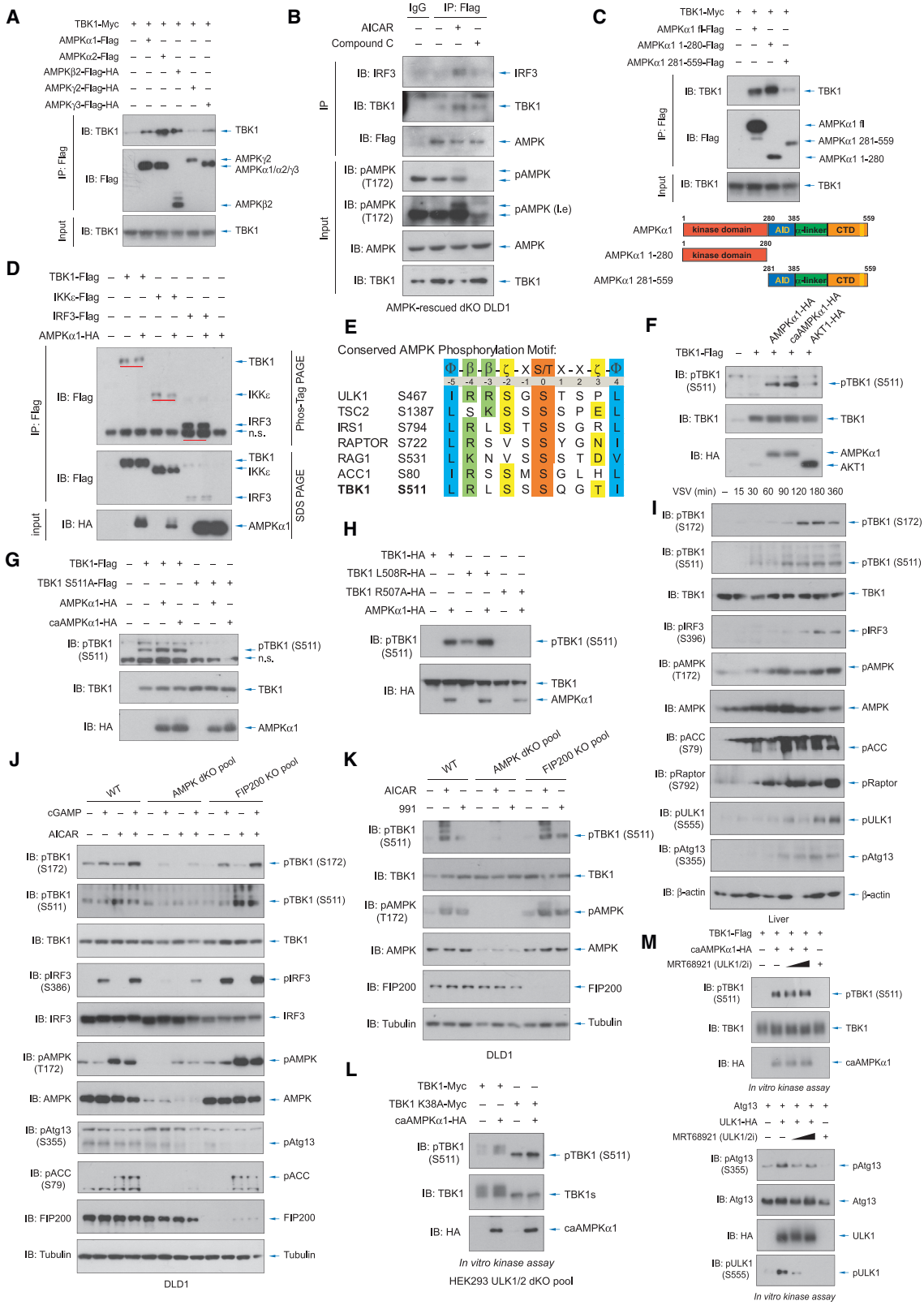

(legend on next page)

Please cite this article in press as: Zhang et al., AMPK directly phosphorylates TBK1 to integrate glucose sensing into innate immunity, Molecular Cell (2022), https://doi.org/10.1016/j.molcel.2022.10.026

phosphorylation at S511 (Figure 4J, 4K, and S4H), which was induced by AICAR or 991, another specific AMPK activator.[80] An *in vitro* kinase assay using AMPKα1 and TBK1 separately expressed and purified from ULK1/2 dKO HEK293 cells revealed that AMPKα1 directly phosphorylated TBK1 at this S511 residue (Figure 4L), a process that did not affect by ULK1/2 inhibition (Figure 4M). TBK1 is auto-phosphorylated at S172 and activated during overexpression. However, TBK1 failed to phosphorylate themselves at S511 (Figure S4I). These intriguing data suggest that TBK1 is a new substrate of AMPK, directly modifying at a classic AMPK substrate motif.

TBK1 phosphorylation by AMPK facilitates antiviral signalosome assembly

The biological importance of the AMPK-TBK1 axis is further investigated. We detected the elevated level of TBK1 activation when TBK1 was coexpressed with AMPKα1 or its kinase domain, indicated by phospho-TBK1 S172 levels and somewhat slower mobility shift in Phos-tag PAGE (Figure 5A). An *in vitro* kinase assay revealed that TBK1, when cotransfected with active AMPK, exhibited an increased efficacy to phosphorylate IRF3 (Figure 5B). Using the S511E/D mutants to mimic AMPK-phosphorylated TBK1 and the S511A mutant disrupts AMPK-mediated modification, we found that preventing AMPK-mediated phosphorylation compromised TBK1-IRF3 signaling while mimicking this phosphorylation increased it (Figure 5C). Intriguingly, a distinct and opposite effect was revealed between phosphorylation of S511 and S510 (Figures 5C and 5D), which was mediated by AKT1 (Figure S4E and Wu et al.[44]), indicating subtle regulations on TBK1 from two critical kinases represent catabolic and anabolic functions, respectively. The observation was further supported by their distinct effects on modifications at the proximal residues in phosphorylation-rich motifs (PRMs), such as S499, T517, and S518 residues (Figure S5A). These data suggest that AMPK-mediated TBK1 phosphorylation at S511 facilitates antiviral signaling.

To characterize its biological effect, we successfully generated via CRISPR-Cas9 technique a few DLD1 knockin (KI) homogeneous clones that prevented (S511A) or mimicked (S511D) AMPK-mediated phosphorylation (Figures S5B and S5C). Viral RNA sensing or STING signaling was attenuated when endogenous TBK1 was mutated to disrupt AMPK modification (Figures 5E and 5F), in sharp contrast to TBK1 mutant resisting AKT1 modification. Conversely, when endogenous TBK1 mimicked AMPK-mediated phosphorylation (S511D KI), an enhanced STING signaling level was detected (Figures 5G and S5D). Notably, this signal was comparable to the conditions with AMPK activation, and AICAR-enhanced activation effect was lost (Figure 5G). These consistent data suggest a central role of AMPK-mediated phosphorylation at TBK1 S511 in coupling glucose and nucleic acid sensing.

We next attempted to understand the precise alterations in signaling caused by this specific TBK1 phosphorylation. Intriguingly, the weak interaction between TBK1 and IRF3, critical for STING and MAVS signalosome assembly, was strikingly enhanced by AMPKα or AMPK activators but not ULK1 (Figures 5H and S5E). We detected a compromised interaction between TBK1 S511A and IRF3, compared with an enhanced association between TBK1 S511D and IRF3 (Figures 5I and S5F). Remarkably, we even detected an interaction between stably expressed TBK1 and endogenous IRF3 in gut epithelial cells upon AICAR treatment (Figure 5J), the molecular event known for being extraordinarily transient and impossible to visualize. The interactions between TBK1 with STING or MAVS, vital for signalosome assembly, were similarly enhanced by AMPK, albeit moderately (Figures 5K and S5G). In addition, we observed in TBK1 S511A KI cells than in TBK1 S511D KI cells the slower dynamic of endogenous STING aggregation (Figure 5L), a process representing STING signalosome assembly.[44] Besides, AMPK

Figure 4. AMPK directly phosphorylates TBK1 at the S511 residue

(A) The association between TBK1 and the α or β subunit of AMPK was detected by coimmunoprecipitation.

(B) Flag-tagged AMPKα1 was stably reconstituted into AMPK-dKO DLD1 cells, and its association with endogenous TBK1 was evaluated by coimmunoprecipitation to overcome the unavailability of an AMPK antibody for immunoprecipitation. Visible associations between AMPKα1 and endogenous TBK1 and IRF3 were detected, particularly in the presence of AICAR.

(C) Domain mapping analyses using the indicated AMPKα1 truncations revealed an affinity of the kinase domain (a.a. 1–280) of AMPKα1 for TBK1 interaction.

(D) Phos-Tag electrophoresis, which exaggerates mobility shifts of phosphorylated proteins, detected an alteration of TBK1, but not that of IKKε or IRF3, in the presence of AMPKα1.

(E) TBK1 sequence proximal to S511 matched the known preferred consensus substrate motif of AMPK, featuring basic and hydrophobic residues at −3 (or −4) and −5, a strong hydrophobic residue at +4, and hydrophilic residues at −2 and +3.

(F and G) A phosphorylation-specific antibody targeting phospho-TBK1 S511 was generated in collaboration with Abcam (F), which recognized AMPK-mediated TBK1 phosphorylation (F and G) and did not react with S511A (G).

(H) AMPKα1 phosphorylated TBK1 wild type and L508R mutant (ULK1 substrate motif is disrupted), but not TBK1 R507 mutant (AMPK substrate motif is disrupted).

(I) Endogenous phospho-TBK1 S511 was rapidly induced upon VSV infection in the murine livers, accompanied sequentially by AMPK activation and the phosphorylation of TBK1 S172, ULK1, and IRF3 phosphorylation.

(J and K) sgRNA-mediated deficiency of AMPKα1/α2, but not FIP200, eliminated AICAR or 991-induced endogenous phospho-TBK1 S511 (J and K) and TBK1 activation (J).

(L) Constitutively active AMPKα1, which was purified from ULK1/2 dKO HEK293 cells, directly phosphorylated WT or kinase-dead (K38A) TBK1 at S511 during *in vitro* kinase assay.

(M) ULK1/2 inhibition by MRT68921 (0.1–1 μM) blocked ULK1-induced phosphorylation of Atg13 *in vitro*, but not AMPKα1-induced phosphorylation of TBK1 at S511.

See also Figure S4.

Please cite this article in press as: Zhang et al., AMPK directly phosphorylates TBK1 to integrate glucose sensing into innate immunity, Molecular Cell (2022), https://doi.org/10.1016/j.molcel.2022.10.026

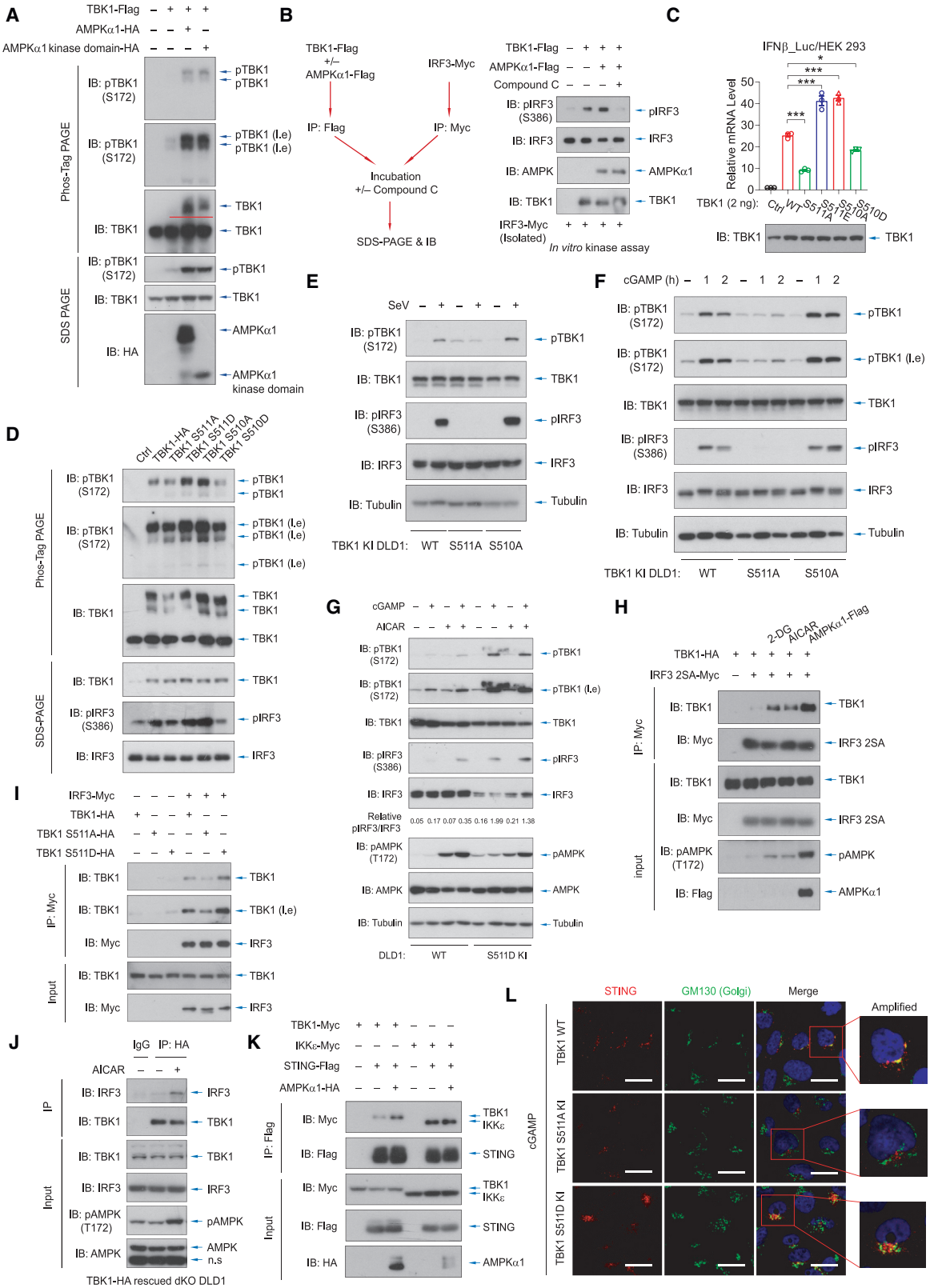

(legend on next page)

Please cite this article in press as: Zhang et al., AMPK directly phosphorylates TBK1 to integrate glucose sensing into innate immunity, Molecular Cell (2022), https://doi.org/10.1016/j.molcel.2022.10.026

appeared to reduce the K48-linked ubiquitination level of TBK1 (Figure S5H). These surprising observations suggest that TBK1 phosphorylation by AMPK facilitates signaling complex assembly via enhanced protein associations.

TBK1 phosphorylation by AMPK is crucial for cellular antiviral defense

We next evaluated the function of AMPK in cellular antiviral defense. Compromised VSV replications were seen in MEFs upon AICAR treatment (Figure 6A) or in gut epithelial cells upon AICAR treatment or glucose deprivation (Figure S6A), as revealed by the GFP tag integrated into the viral genome. Genetic ablation of AMPK α1/α2 weakened antiviral defense in MEFs and abolished the antiviral effect of AICAR (Figure 6A). By contrast, gRNA-mediated deletion/depletion of AMPK α subunits or treatment with Compound C, rather than FIP200 knockout, impeded antiviral resistance in gut epithelial cells and BMDMs, leading to apparent increases in VSV replications (Figures 6B, 6C, and S6B–S6D). HSV-1 replications in gut epithelial cells, similarly assessed by viral genome-integrated GFP, were suppressed when AMPK was activated by AICAR, 991, or metformin, a mild but long-lasting AMPK agonist[81] (Figures 6D and S6E). By contrast, KO of AMPK α subunits aggravated HSV-1 replications (Figure 6E). Additionally, we detected a substantial augmentation for replications of RNA and DNA viruses, rather than viral infection rate, in DLD1 cells where the AMPK-TBK1 axis was disrupted by S511A KI (Figures 6F and S6F). These consistent data suggest that the AMPK-TBK1 axis is vital for cellular antiviral defense due to its potentiation on nucleic acid sensing.

The AMPK-TBK1 axis is critical for innate antiviral immunity in zebrafish and mice

The physiological role of AMPK-TBK1 regulation was first evaluated in zebrafish by an infection model previously developed.[40,75,76] Zebrafish embryos microinjected with VSV displayed a robust enhancement of viral resistance and extended survival when in the AICAR-containing medium (Figure 7A), suggesting a critical role of AMPK in antiviral physiology and its conservation during evolution. We next employed an intriguing and convenient infectious model, the corneal HSV-1 infection, where the scales of HSV-1 infection and disease symptoms can be directly visualized and scored.[44,82] We observed that the ocular administration of AICAR significantly improved viral resistance against HSV-1, with an evident amelioration of infection phenotypes (Figure 7B), ocular disease scores (Figure 7C), and viral loads (Figure 7D). In addition, mice with conditional knockout of AMPKα1/α2 in myeloid cells showed somewhat reduced antiviral responses against VSV and increased viral replication (Figure 7E).

To precisely evaluate the *in vivo* function of the AMPK-TBK1 axis, we generated knockin mice harboring the S511E TBK1 that mimicked AMPK-mediated phosphorylation and the S511A TBK1 that disrupted the AMPK-TBK1 axis, utilizing a CRISPR-mediated strategy (Figures S7A–S7C). The homozygotes of TBK1 S511E mice and TBK1 S511A mice were viable and appeared normal (Figure S7C). Viral RNA sensing was enhanced in PMs isolated from the TBK1 S511E mice but was attenuated in S511A PMs (Figures 7F, 7G, and S7D). Likewise, nucleic acid sensing-induced expression of ISGs and cytokines was markedly increased in TBK1 S511E PMs in response to HSV-1 (Figure 7H), VSV (Figure S7E), SeV (Figure S7F), mitochondrial DNA (mtDNA) leaking (Figure 7I), or RNA analogs (Figure S7G). By contrast, uncoupling the AMPK-TBK1 axis by S511A KI compromised the PMs for sensing cytosolic DNA or RNA (Figures 7J and S7H). Replicates of VSV and HSV-1 were substantially compromised in TBK1 S511E PMs (Figures 7K and 7L), in sharp distinction to an increase of HSV-1 replication in PMs with uncoupled AMPK-TBK1 axis (Figure 7K). Notably, we observed a marked decrease of HSV-1 viral loads in the eyelids of sacrificed TBK1 S511E mice (Figure 7M) and ameliorated phenotypes of ocular disease in the HSV-1 corneal infection model (Figure 7N). These observations suggest that TBK1 phosphorylation at S511 by AMPK is physiologically critical to antiviral responses and immunity.

DISCUSSION

In this report, we revealed an unexpected mechanism by which the primary glucose sensor directly phosphorylates and primes the essential kinase of innate immunity to facilitate invasion surveillance, thus bridging two major sensing systems in living organisms (Figure S7I). This molecular coupling was consistently in cells, tissues, zebrafish, and mice, indicating its ubiquity and

Figure 5. TBK1 phosphorylation by AMPK is vital for antiviral signalosome assembly

(A) Coexpression of AMPKα1 or its N-terminal kinase domain potentiated TBK1 activity, measured by increased TBK1 S172 phosphorylation and slower mobility shift portion in Phos-tag electrophoresis.

(B) AMPK enhanced the capability of TBK1 to phosphorylate IRF3 in an *in vitro* kinase assay, an effect suppressed by Compound C.

(C and D) A significant loss of TBK1 function was recorded in TBK1 decoupling AMPK-mediated phosphorylation (S511A), by the IRF3-responsive reporter (C) or phospho-TBK1 and phospho-IRF3 immunoblottings (D). TBK1 mimicking AMPK-mediated phosphorylation (S511E) displayed a positive role, while TBK1 S510 mutants exhibited an opposite effect to S511 (C and D).

(E and F) RNA sensing (E) or STING signaling (F), stimulated by SeV infection or cGAMP treatment and evidenced by TBK1 and IRF3 activation, was largely lost in cells containing TBK1 S511A KI homozygotes but increased in TBK1 mutant uncoupling with AKT1 modification (E).

(G) The S511D KI DLD1 cells showed a robust increase in cGAMP-stimulated DNA sensing signaling and were unresponsive to AICAR.

(H and I) A weak interaction between TBK1 and IRF3 was captured by coimmunoprecipitation using an IRF3 2SA mutant. Coexpression of AMPKα1 or activation of AMPK by 2-DG and AICAR profoundly enhanced this association (H), while TBK1 S511A and S511D showed opposite effects in IRF3 interaction (I).

(J) The transient interaction between endogenous IRF3 and stably expressed TBK1 was unexpectedly detected in the presence of AICAR.

(K) AMPKα1 coexpression facilitated the interaction between TBK1 and STING while failing to enhance the interaction between STING and IKKε.

(L) cGAMP-induced assembly of the endogenous STING signalosome in DLD1 cells was revealed by STING puncta under immunofluorescence, weakened in TBK1 S511A KI cells but strengthened in S511D KI cells. Scale bars, 20 μm.

See also Figure S5.

Please cite this article in press as: Zhang et al., AMPK directly phosphorylates TBK1 to integrate glucose sensing into innate immunity, Molecular Cell (2022), https://doi.org/10.1016/j.molcel.2022.10.026

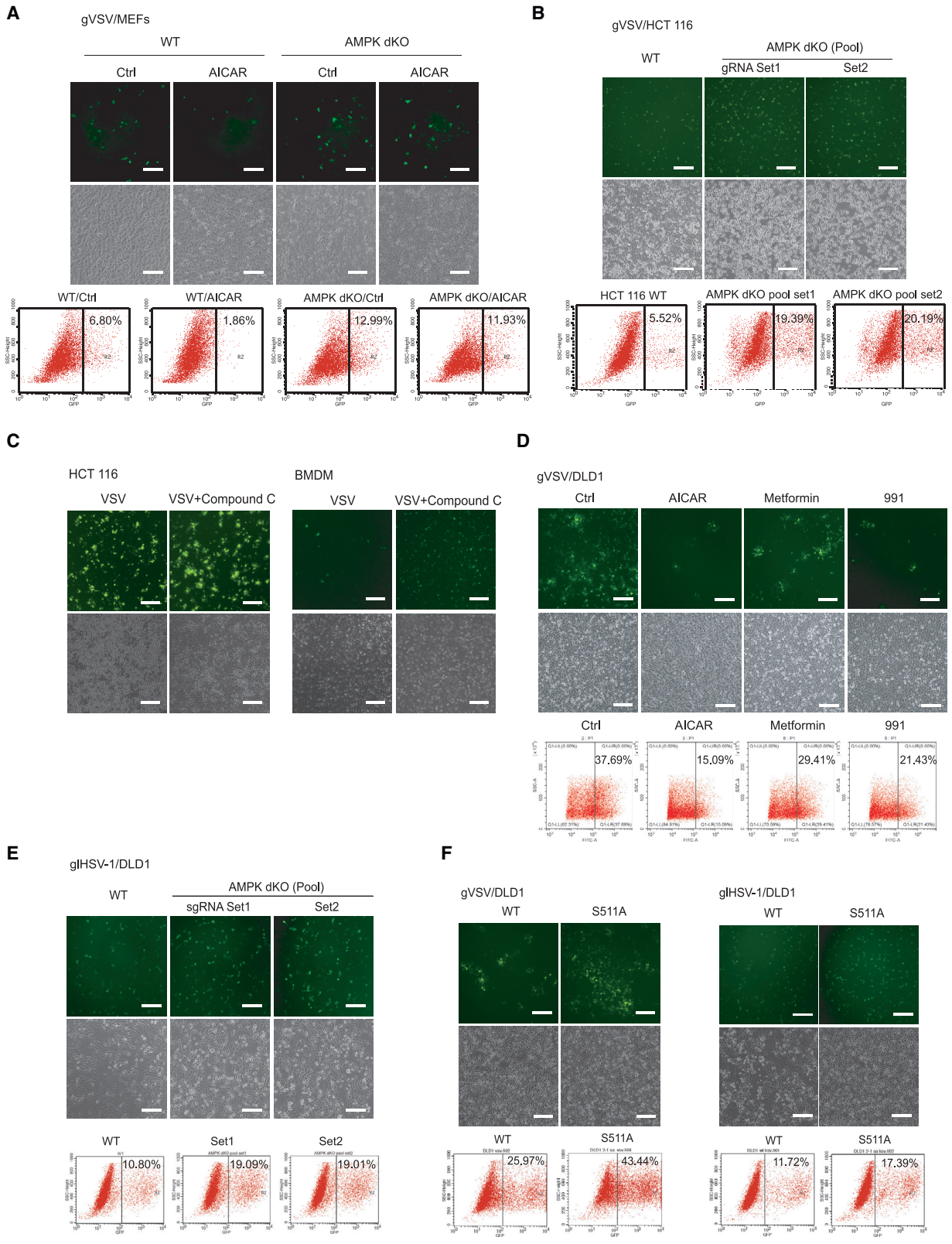

(legend on next page)

Please cite this article in press as: Zhang et al., AMPK directly phosphorylates TBK1 to integrate glucose sensing into innate immunity, Molecular Cell (2022), https://doi.org/10.1016/j.molcel.2022.10.026

high evolutionary conservation. Besides, we observed a physiological phenomenon that is highly intriguing: a rapid and dramatic drop in blood glucose levels upon the early stage of viral infection. The findings demonstrate the importance of a regulated glucose deficiency in innate immunity.

As the ancestral role of AMPK in glucose sensing,[49] AMPK activates at the lysosomal surface in response to decreasing glucose levels through the interplay between aldolase and the v-ATPase-Ragulator complex.[50,51] Undoubtedly, the AMPK-TBK1 axis adds a crucial role of AMPK in innate immunity, beyond its classical roles in glucose and lipid metabolism, protein synthesis, autophagy, and mitochondrial physiology.[48] The observations also change our prevailing view of metabolic integration in innate immunity and host-pathogen interactions. Because the imbalance in innate nucleic acid sensing is a leading cause of autoimmune and autoinflammatory diseases,[83,84] the involvement of glucose deficiency and AMPK in these conditions is worth further investigation.

Notably, we observed a rapid and dramatic drop in blood glucose levels in various species of rodents upon the early stage of viral infection, demonstrating a physiological but previously unappreciated link between microbial sensing and glucose sensing. The drop in blood glucose level and activation of AMPK in mice was very rapid, in sharp distinction to the slow alteration of blood glucose levels caused by food intake during long-term IAV infection,[70] which might represent an acute versus long-term phase of physiological responses upon viral infection. Dramatic alteration in blood glucose levels is viral nucleic acid dependence and humoral immunity independence and might involve the complex interactions between PRRs and the nervous system[70] and the role of TBK1 in cellular glycolysis,[68,69] but undetermined yet.

Pathogenic nucleic acids from the invading microbes or injured cellular organelles are sensed in the cytosol by RIG-I-like receptors and cGAS.[2,4] TBK1 is central during the assembly and activation of MAVS and STING signalosomes and the transmission of invasion signal to IRF3, assumed to be activated by transphosphorylation at S172 and sequentially phosphorylates MAVS/STING and IRF3.[5,18,19,85,86] We reveal that AMPK is associated with TBK1 during its activation and directly phosphorylates TBK1 at S511. Simulating this exact AMPK-mediated phosphorylation on S511 in cells or animals caused TBK1 to tether with IRF3 with an extremely high affinity. By contrast, genetic or pharmacologic targeting of AMPK or point mutagenesis of TBK1 S511 by knockin strategies attenuates both STING and MAVS signalosomes, leading to a substantial loss of IRF3 activation. A recent report indicates an AMPK-ULK1-TBK1 axis that ULK1 phosphorylates TBK1 at S172 residue in adipocytes,[59] which differs from our observation in innate immune systems. Knockin strategies in TBK1, point mutagenesis of AMPK substrate motif, genetic or pharmacological ablation of ULK1/2 kinases, and *in vitro* kinase assays all suggest a direct AMPK-TBK1 axis by which AMPK directly phosphorylates TBK1 at S511, independent of ULK kinases. Intriguingly, we noticed a dramatic difference in phosphorylation between TBK1 S510 (by AKT1) and S511 (by AMPK), which has distinct effects on the phosphorylation at proximal residues. For instance, phospho-TBK1 S499 is severely suppressed by AKT1[44] but substantially enhanced by AMPK. The suppression of AKT1 activity increases TBK1 S511 phosphorylation (Figure S4E and Wu et al.[44]), implying an opposing role of AKT1 and AMPK on TBK1. These observations reflect a molecular switching role of this TBK1 phosphorylation-rich motif (PRM) segment, controlled by subtle modifications and possible regulator binding. However, it is currently unknown how this specific interface in the TBK1 coiled-coil domain 1 (CCD1) participates in IRF3 recruitment. Recent structural studies on the STING-TBK1 complex[19,86,87] suggest the PRM is located at a long α helix and short loop, which may comprise a potential interaction interface between the TBK1 dimers, or with other regulators.

Identifying various AMPK substrates by decoding the AMPK substrate motif has significantly expanded our knowledge about this central controller of metabolism.[77,79] Profoundly, the amino acid sequence of TBK1 proximal to S511 perfectly matched the classic AMPK substrate motif, including the hydrophobic residues at −5 (L) and +4 (I) and a basic residue at −3 or −4 (R), and a polar side chain at +3 (T) and a neutral polar residue at −2 (S), important in substrate recognition and modification.[77] Furthermore, the AMPK substrate motif features on TBK1 are highly evolutionarily conserved among almost all vertebrates. Conversely, the S510 residue in the PRM segment is the one for AKT1 modification[44] instead of AMPK, lacking all the essential features for the AMPK substrate motif except a basic residue at −3 (R). We detected a robust signal for AMPK-directed modification at S511 via mass spectrometry analyses and with an antibody explicitly targeting the phosphorylated residue in cells, *in vitro*, and endogenous TBK1 upon AMPK activation. Collectively, these consistent observations identify TBK1 as a direct and physiological substrate of AMPK. As the central kinase in innate immunity and cellular stress response,[36] TBK1 probably also regulates the activities of AMPK and mTOR[59,88] and in a context-dependent manner, which may form feedbacks to control the innate immune signaling pathways.

In conclusion, our study reveals a critical role of AMPK-mediated TBK1 phosphorylation at S511 to prime the glucose-scaled

Figure 6. AMPK facilitates cellular antiviral defense

(A) Cellular resistance to the GFP-tagged RNA virus VSV was assessed by microscopy (top) or FACS (bottom) in cells with viral replication (GFP^+ cells), revealing impaired antiviral resistance in MEFs without AMPKα1/α2. Scale bars, 100 μm.

(B and C) gRNA-mediated deletion/depletion of AMPK (B) or Compound C treatment (C) weakened antiviral resistance of HCT116 cells and BMDMs. Scale bars, 100 μm.

(D) Activation of AMPK by AICAR, 991, or metformin improved cellular resistance of DLD1 to the RNA virus VSV, as revealed by microscopy and FACS. Scale bars, 100 μm.

(E) gRNA-mediated knockout/knockdown of AMPKα1/α2 in DLD1 cells decreased their antiviral resistance against HSV-1. Scale bars, 100 μm.

(F) Antiviral resistance against VSV or HSV-1 was dampened in cells with disruption of the AMPK-TBK1 axis (TBK1 S511A KI). Scale bars, 100 μm.

See also Figure S6.

Please cite this article in press as: Zhang et al., AMPK directly phosphorylates TBK1 to integrate glucose sensing into innate immunity, Molecular Cell (2022), https://doi.org/10.1016/j.molcel.2022.10.026

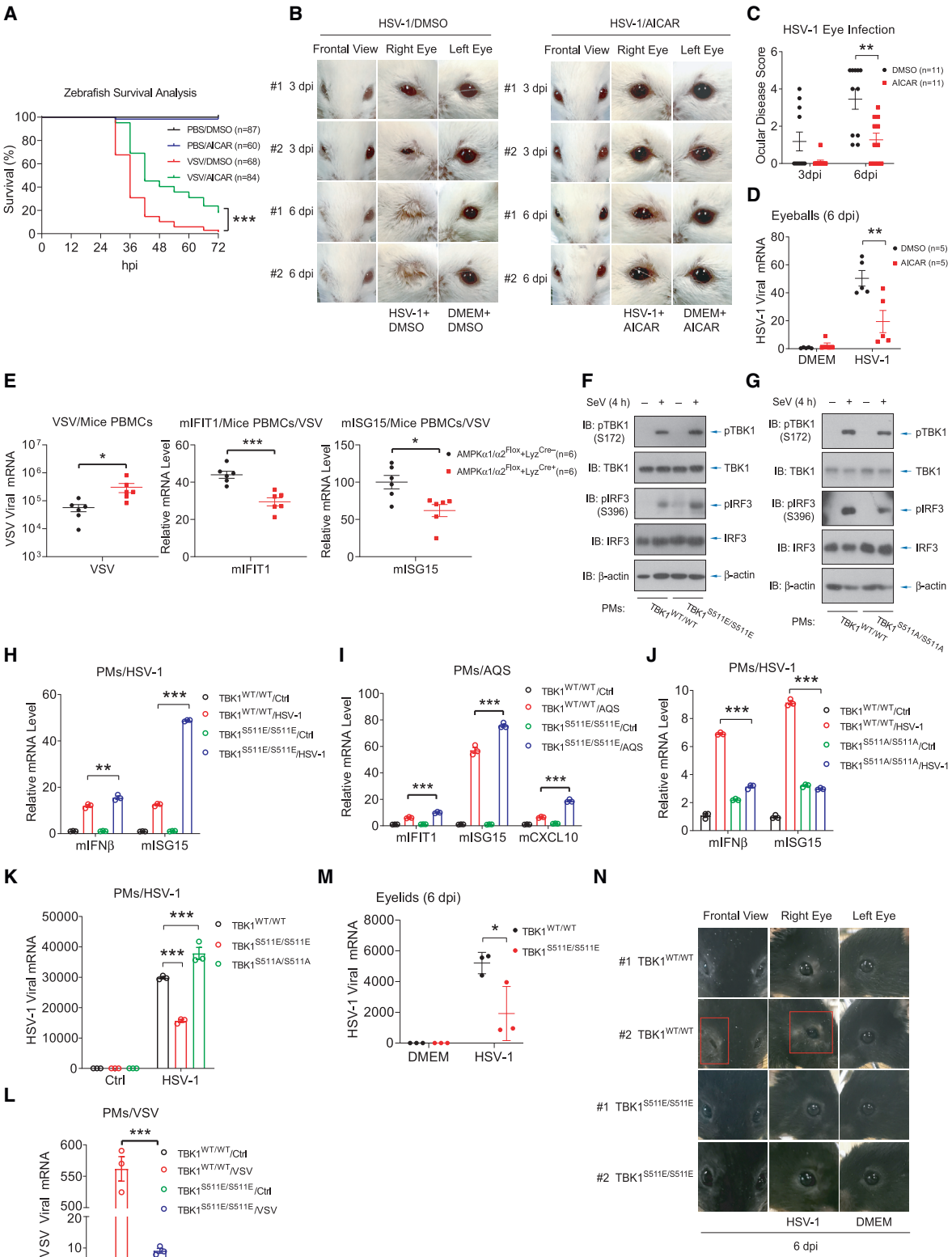

(legend on next page)

immune response, thus connecting glucose metabolism to innate immunity in a direct and elegant pathway. We suggest that AMPK activation, caused by a physiological response to the early stage of viral infection, dictates the magnitude of innate antiviral immunity. Therefore, the pharmacological manipulation of AMPK, which looks feasible, may offer potential therapeutic benefits for treating infectious diseases.

Limitations of the study

Although our data report a rapid and dramatic drop in blood glucose, the underlying mechanism of this alteration and the precise glucose level within various tissues are undetermined. This report also remains unanswered about how this AMPK-TBK1 axis impacts other physiological events mediated by MAVS and STING, such as autoimmune diseases and cancer immunology.

STAR★METHODS

Detailed methods are provided in the online version of this paper and include the following:

- KEY RESOURCES TABLE
- RESOURCE AVAILABILITY
  - Lead contact
  - Materials availability
  - Data and code availability
- EXPERIMENTAL MODEL AND SUBJECT DETAILS
  - Mice
  - Zebrafish
  - Peritoneal Macrophages
  - Cell Lines
  - Intestinal Organoids
  - Viruses
- METHOD DETAILS
  - Expression Plasmids, Viruses, Reagents, and Antibodies
  - Plasmids Transfection and Virus Infection of Cultured Cells
  - CRISPR/Cas9-mediated Generation of AMPKα1/α2$^{-/-}$, ULK1/2$^{-/-}$, FIP200$^{-/-}$ and TBK1 Knock-in Cells
  - Luciferase Reporter Assay
  - Quantitative RT-PCR Assay
  - Coimmunoprecipitations and Immunoblottings
  - *In vitro* Kinase Assay
  - Immunofluorescence, Microscopy, and FACS
  - VSV Challenge in Zebrafish
  - Blood Glucose Level Measurement and Viral Challenge in Mice
  - Murine Corneal HSV-1 Infection
  - Nano-liquid Chromatography/Tandem MS (Nano LC-MS/MS) Analysis
  - CE-MS-based Measurement of AMP, ADP, and ATP
  - GC-MS-based Measurement of Long-Chain Fatty Acids (LCFAs)
- QUANTIFICATION AND STATISTICAL ANALYSIS

SUPPLEMENTAL INFORMATION

Supplemental information can be found online at https://doi.org/10.1016/j.molcel.2022.10.026.

ACKNOWLEDGMENTS

This research was sponsored by the National Key Research and Development Program of China (2021YFA1301401 to P.X. and 2021YFD1801103 to Q.Z.) and the NSFC projects (31725017 and 31830052 to P.X. and 82271768 and 81902915 to Q.Z.). We are grateful to Drs. Jiahuai Han and Zhengfan Jiang for HSV-1 and VSV viruses, Michiyuki Matsuda for AMPKAR-EV mice, Mingxia Zhu and Cixiong Zhang (Xiamen University) for technical assistance, and Yan Jessie Zhang (UT Austin) for helpful discussions. Thanks also to technical assistance by the Life Sciences Institute core facilities, Zhejiang University.

AUTHOR CONTRIBUTIONS

Q.Z. and S.L. carried out most experiments. C.-S.Z., Q.W., X.Y., F.M., R.Z., A.W., S.C., and F.Z. contributed to several experiments, and X.W., L.L., J.H., Y.-W.H., J.Z., J.Q., X.-H.F., T.L. and S.-C.L. helped with data analyses and discussions. P.X. and Q.Z. conceived the study and experimental design, and P.X. wrote the manuscript.

DECLARATION OF INTERESTS

The authors declare no competing interests.

Received: October 13, 2021
Revised: May 18, 2022
Accepted: October 25, 2022
Published: November 15, 2022

Figure 7. The AMPK-TBK1 axis is critical for antiviral immunity

(A) gVSV was microinjected into the yolks of zebrafish embryos (48 hpf) to elicit a robust viral infection state, which eventually led to the death of zebrafish embryos starting at 24–30 hpi. Antiviral immunity against VSV infection was evaluated in embryos upon AICAR treatment. *** $p < 0.001$, by log-rank test.

(B–D) Corneal HSV-1 infection in BALB/c mice was performed, and the severity of ocular disease symptoms such as eyelid swelling, eye closure, and eye crusting are shown in representative images (B) and was assessed by disease scoring (C), with or without AICAR administration. RT-qPCR was performed to detect HSV-1 viral mRNA in the eyeballs of sacrificed mice at 6 dpi.

(E) VSV challenges in mice with conditional knockout of AMPKα1/α2 in the myeloid line (Lyz^{Cre}) revealed enhanced replications of VSV and compromised antiviral responses in PBMCs, as revealed by the mRNA expression ISGs and viral genome.

(F and G) PMs isolated from TBK1$^{S511E/S511E}$ or TBK1$^{S511A/S511A}$ KI mice exhibited an enhanced or attenuated activation of endogenous TBK1 and IRF3 upon SeV infection, respectively.

(H–J) PMs of TBK1$^{S511E/S511E}$ KI mice exhibited increases in ISGs mRNA expression in response to HSV-1 infection (H) or mitochondrial DNAs (mtDNAs) leaking (I), in contradiction to TBK1$^{S511A/S511A}$ PMs (J).

(K and L) Replicates of HSV-1 (K) or VSV (L) were substantially lower when infected in PMs from TBK1$^{S511E/S511E}$ KI mice, in contrast to PMs from WT or TBK1$^{S511A/S511A}$ KI mice.

(M and N) Corneal HSV-1 infection in WT or TBK1$^{S511E/S511E}$ KI mice indicated reduced viral loads in TBK1$^{S511E/S511E}$ KI mice in the eyelids at 6 dpi (M) and less severity of ocular disease symptoms (N).

See also Figure S7.

REFERENCES

1. Ma, J., Chen, T., Wu, S., Yang, C., Bai, M., Shu, K., Li, K., Zhang, G., Jin, Z., He, F., et al. (2019). iProX: an integrated proteome resource. Nucleic Acids Res. *47*, D1211–D1217. https://doi.org/10.1093/nar/gky869.
2. Yoneyama, M., Kikuchi, M., Natsukawa, T., Shinobu, N., Imaizumi, T., Miyagishi, M., Taira, K., Akira, S., and Fujita, T. (2004). The RNA helicase RIG-I has an essential function in double-stranded RNA-induced innate antiviral responses. Nat. Immunol. *5*, 730–737. https://doi.org/10.1038/ni1087.
3. Gao, P., Ascano, M., Wu, Y., Barchet, W., Gaffney, B.L., Zillinger, T., Serganov, A.A., Liu, Y., Jones, R.A., Hartmann, G., et al. (2013). Cyclic [G(2′,5′)pA(3′,5′)p] is the metazoan second messenger produced by DNA-activated cyclic GMP-AMP synthase. Cell *153*, 1094–1107. https://doi.org/10.1016/j.cell.2013.04.046.
4. Sun, L., Wu, J., Du, F., Chen, X., and Chen, Z.J. (2013). Cyclic GMP-AMP synthase is a cytosolic DNA sensor that activates the type I interferon pathway. Science *339*, 786–791. https://doi.org/10.1126/science.1232458.
5. Chen, Q., Sun, L., and Chen, Z.J. (2016). Regulation and function of the cGAS-STING pathway of cytosolic DNA sensing. Nat. Immunol. *17*, 1142–1149. ni.3558. https://doi.org/10.1038/ni.3558.
6. Takeuchi, O., and Akira, S. (2010). Pattern recognition receptors and inflammation. Cell *140*, 805–820. https://doi.org/10.1016/j.cell.2010.01.022.
7. Roers, A., Hiller, B., and Hornung, V. (2016). Recognition of endogenous nucleic acids by the innate immune system. Immunity *44*, 739–754. S1074-7613(16)30107-8. https://doi.org/10.1016/j.immuni.2016.04.002.
8. Hu, M.M., and Shu, H.B. (2020). Innate immune response to cytoplasmic DNA: mechanisms and diseases. Annu. Rev. Immunol. *38*, 79–98. https://doi.org/10.1146/annurev-immunol-070119-115052.
9. Rehwinkel, J., and Gack, M.U. (2020). RIG-I-like receptors: their regulation and roles in RNA sensing. Nat. Rev. Immunol. *20*, 537–551. https://doi.org/10.1038/s41577-020-0288-3.
10. Chen, S., Liu, S., Wang, J., Wu, Q., Wang, A., Guan, H., Zhang, Q., Zhang, D., Wang, X., Song, H., et al. (2020). TBK1-mediated DRP1 targeting confers nucleic acid sensing to reprogram mitochondrial dynamics and physiology. Mol. Cell *80*, 810–827.e7. https://doi.org/10.1016/j.molcel.2020.10.018.
11. Ablasser, A., Goldeck, M., Cavlar, T., Deimling, T., Witte, G., Röhl, I., Hopfner, K.P., Ludwig, J., and Hornung, V. (2013). cGAS produces a 2′-5′-linked cyclic dinucleotide second messenger that activates STING. Nature *498*, 380–384. nature12306. https://doi.org/10.1038/nature12306.
12. Wu, J., Sun, L., Chen, X., Du, F., Shi, H., Chen, C., and Chen, Z.J. (2013). Cyclic GMP-AMP is an endogenous second messenger in innate immune signaling by cytosolic DNA. Science *339*, 826–830. https://doi.org/10.1126/science.1229963.
13. Zhang, X., Shi, H., Wu, J., Zhang, X., Sun, L., Chen, C., and Chen, Z.J. (2013). Cyclic GMP-AMP containing mixed phosphodiester linkages is an endogenous high-affinity ligand for STING. Mol. Cell *51*, 226–235. https://doi.org/10.1016/j.molcel.2013.05.022.
14. Ishikawa, H., and Barber, G.N. (2008). STING is an endoplasmic reticulum adaptor that facilitates innate immune signalling. Nature *455*, 674–678. https://doi.org/10.1038/nature07317.
15. Zhong, B., Yang, Y., Li, S., Wang, Y.Y., Li, Y., Diao, F., Lei, C., He, X., Zhang, L., Tien, P., and Shu, H.B. (2008). The adaptor protein MITA links virus-sensing receptors to IRF3 transcription factor activation. Immunity *29*, 538–550. https://doi.org/10.1016/j.immuni.2008.09.003.
16. Sun, W., Li, Y., Chen, L., Chen, H., You, F., Zhou, X., Zhou, Y., Zhai, Z., Chen, D., and Jiang, Z. (2009). Eris, an endoplasmic reticulum IFN stimulator, activates innate immune signaling through dimerization. Proc. Natl. Acad. Sci. USA *106*, 8653–8658. 0900850106. https://doi.org/10.1073/pnas.0900850106.
17. Zhang, D., Liu, Y., Zhu, Y., Zhang, Q., Guan, H., Liu, S., Chen, S., Mei, C., Chen, C., Liao, Z., et al. (2022). A non-canonical cGAS-STING-PERK pathway facilitates the translational program critical for senescence and organ fibrosis. Nat. Cell Biol. *24*, 766–782. https://doi.org/10.1038/s41556-022-00894-z.
18. Liu, S., Cai, X., Wu, J., Cong, Q., Chen, X., Li, T., Du, F., Ren, J., Wu, Y.T., Grishin, N.V., and Chen, Z.J. (2015). Phosphorylation of innate immune adaptor proteins MAVS, STING, and TRIF induces IRF3 activation. Science *347*, aaa2630. https://doi.org/10.1126/science.aaa2630.
19. Zhang, C., Shang, G., Gui, X., Zhang, X., Bai, X.C., and Chen, Z.J. (2019). Structural basis of STING binding with and phosphorylation by TBK1. Nature *567*, 394–398. https://doi.org/10.1038/s41586-019-1000-2.
20. Sharma, S., tenOever, B.R., Grandvaux, N., Zhou, G.P., Lin, R., and Hiscott, J. (2003). Triggering the interferon antiviral response through an IKK-related pathway. Science *300*, 1148–1151. https://doi.org/10.1126/science.1081315.
21. Fitzgerald, K.A., McWhirter, S.M., Faia, K.L., Rowe, D.C., Latz, E., Golenbock, D.T., Coyle, A.J., Liao, S.M., and Maniatis, T. (2003). IKKepsilon and TBK1 are essential components of the IRF3 signaling pathway. Nat. Immunol. *4*, 491–496. https://doi.org/10.1038/ni921.
22. Chan, Y.K., and Gack, M.U. (2015). RIG-I-like receptor regulation in virus infection and immunity. Curr. Opin. Virol. *12*, 7–14. S1879-6257(15)00005-X. https://doi.org/10.1016/j.coviro.2015.01.004.
23. Zhang, Q., Chen, C., Xia, B., and Xu, P. (2022). Chemical regulation of the cGAS-STING pathway. Curr. Opin. Chem. Biol. *69*, 102170. https://doi.org/10.1016/j.cbpa.2022.102170.
24. Wild, P., Farhan, H., McEwan, D.G., Wagner, S., Rogov, V.V., Brady, N.R., Richter, B., Korac, J., Waidmann, O., Choudhary, C., et al. (2011). Phosphorylation of the autophagy receptor optineurin restricts Salmonella growth. Science *333*, 228–233. https://doi.org/10.1126/science.1205405.
25. Pilli, M., Arko-Mensah, J., Ponpuak, M., Roberts, E., Master, S., Mandell, M.A., Dupont, N., Ornatowski, W., Jiang, S., Bradfute, S.B., et al. (2012). TBK-1 promotes autophagy-mediated antimicrobial defense by controlling autophagosome maturation. Immunity *37*, 223–234. https://doi.org/10.1016/j.immuni.2012.04.015.
26. Gui, X., Yang, H., Li, T., Tan, X., Shi, P., Li, M., Du, F., and Chen, Z.J. (2019). Autophagy induction via STING trafficking is a primordial function of the cGAS pathway. Nature *567*, 262–266. https://doi.org/10.1038/s41586-019-1006-9.
27. Dou, Z., Ghosh, K., Vizioli, M.G., Zhu, J., Sen, P., Wangensteen, K.J., Simithy, J., Lan, Y., Lin, Y., Zhou, Z., et al. (2017). Cytoplasmic chromatin triggers inflammation in senescence and cancer. Nature *550*, 402–406. nature24050. https://doi.org/10.1038/nature24050.
28. Yang, H., Wang, H., Ren, J., Chen, Q., and Chen, Z.J. (2017). cGAS is essential for cellular senescence. Proc. Natl. Acad. Sci. USA *114*, E4612–E4620. 1705499114. https://doi.org/10.1073/pnas.1705499114.
29. Glück, S., Guey, B., Gulen, M.F., Wolter, K., Kang, T.W., Schmacke, N.A., Bridgeman, A., Rehwinkel, J., Zender, L., and Ablasser, A. (2017). Innate immune sensing of cytosolic chromatin fragments through cGAS promotes senescence. Nat. Cell Biol. *19*, 1061–1070. ncb3586. https://doi.org/10.1038/ncb3586.
30. Mackenzie, K.J., Carroll, P., Martin, C.A., Murina, O., Fluteau, A., Simpson, D.J., Olova, N., Sutcliffe, H., Rainger, J.K., Leitch, A., et al. (2017). cGAS surveillance of micronuclei links genome instability to innate immunity. Nature *548*, 461–465. nature23449. https://doi.org/10.1038/nature23449.
31. Meng, F., Yu, Z., Zhang, D., Chen, S., Guan, H., Zhou, R., Wu, Q., Zhang, Q., Liu, S., Venkat Ramani, M.K., et al. (2021). Induced phase separation of mutant NF2 imprisons the cGAS-STING machinery to abrogate antitumor immunity. Mol. Cell *81*, 4147–4164.e7. https://doi.org/10.1016/j.molcel.2021.07.040.
32. Xu, P., Bailey-Bucktrout, S., Xi, Y., Xu, D., Du, D., Zhang, Q., Xiang, W., Liu, J., Melton, A., Sheppard, D., et al. (2014). Innate antiviral host defense

attenuates TGF-beta function through IRF3-mediated suppression of Smad signaling. Mol. Cell *56*, 723–737. https://doi.org/10.1016/j.molcel.2014.11.027.

33. Petrasek, J., Iracheta-Vellve, A., Csak, T., Satishchandran, A., Kodys, K., Kurt-Jones, E.A., Fitzgerald, K.A., and Szabo, G. (2013). STING-IRF3 pathway links endoplasmic reticulum stress with hepatocyte apoptosis in early alcoholic liver disease. Proc. Natl. Acad. Sci. USA *110*, 16544–16549. https://doi.org/10.1073/pnas.1308331110.

34. Cerboni, S., Jeremiah, N., Gentili, M., Gehrmann, U., Conrad, C., Stolzenberg, M.C., Picard, C., Neven, B., Fischer, A., Amigorena, S., et al. (2017). Intrinsic antiproliferative activity of the innate sensor STING in T lymphocytes. J. Exp. Med. *214*, 1769–1785. jem.20161674. https://doi.org/10.1084/jem.20161674.

35. Melki, I., Rose, Y., Uggenti, C., Van Eyck, L., Frémond, M.L., Kitabayashi, N., Rice, G.I., Jenkinson, E.M., Boulai, A., Jeremiah, N., et al. (2017). Disease-associated mutations identify a novel region in human STING necessary for the control of type I interferon signaling. J. Allergy Clin. Immunol. *140*, 543–552.e5. S0091-6749(16)31438-5. https://doi.org/10.1016/j.jaci.2016.10.031.

36. Zhou, R., Zhang, Q., and Xu, P. (2020). TBK1, a central kinase in innate immune sensing of nucleic acids and beyond. Acta Biochim. Biophys. Sin. (Shanghai) *52*, 757–767. https://doi.org/10.1093/abbs/gmaa051.

37. Hou, F., Sun, L., Zheng, H., Skaug, B., Jiang, Q.X., and Chen, Z.J. (2011). MAVS forms functional prion-like aggregates to activate and propagate antiviral innate immune response. Cell *146*, 448–461. S0092-8674(11)00716-1. https://doi.org/10.1016/j.cell.2011.06.041.

38. Porritt, R.A., and Hertzog, P.J. (2015). Dynamic control of type I IFN signalling by an integrated network of negative regulators. Trends Immunol. *36*, 150–160. S1471-4906(15)00018-6. https://doi.org/10.1016/j.it.2015.02.002.

39. Liu, J., Qian, C., and Cao, X. (2016). Post-translational modification control of innate immunity. Immunity *45*, 15–30. S1074-7613(16)30242-4. https://doi.org/10.1016/j.immuni.2016.06.020.

40. Zhang, Q., Meng, F., Chen, S., Plouffe, S.W., Wu, S., Liu, S., Li, X., Zhou, R., Wang, J., Zhao, B., et al. (2017). Hippo signalling governs cytosolic nucleic acid sensing through YAP/TAZ-mediated TBK1 blockade. Nat. Cell Biol. *19*, 362–374. https://doi.org/10.1038/ncb3496.

41. Abe, H., Satoh, J., Shirasaka, Y., Kogure, A., Kato, H., Ito, S., and Fujita, T. (2020). Priming Phosphorylation of TANK-binding kinase 1 by IF06BB kinase F062 is essential in toll-like receptor 3/4 signaling. Mol. Cell. Biol. *40*. https://doi.org/10.1128/MCB.00509-19.

42. Liu, S., Chen, S., Li, X., Wu, S., Zhang, Q., Jin, Q., Hu, L., Zhou, R., Yu, Z., Meng, F., et al. (2017). Lck/Hck/Fgr-mediated tyrosine phosphorylation negatively regulates TBK1 to restrain innate antiviral responses. Cell Host Microbe *21*, 754–768.e5. https://doi.org/10.1016/j.chom.2017.05.010.

43. Li, X., Yang, M., Yu, Z., Tang, S., Wang, L., Cao, X., and Chen, T. (2017). The tyrosine kinase Src promotes phosphorylation of the kinase TBK1 to facilitate type I interferon production after viral infection. Sci. Signal. *10*. https://doi.org/10.1126/scisignal.aae0435.

44. Wu, S., Zhang, Q., Zhang, F., Meng, F., Liu, S., Zhou, R., Wu, Q., Li, X., Shen, L., Huang, J., et al. (2019). HER2 recruits AKT1 to disrupt STING signalling and suppress antiviral defence and antitumour immunity. Nat. Cell Biol. *21*, 1027–1040. https://doi.org/10.1038/s41556-019-0352-z.

45. Zhu, L., Li, Y., Xie, X., Zhou, X., Gu, M., Jie, Z., Ko, C.J., Gao, T., Hernandez, B.E., Cheng, X., and Sun, S.C. (2019). TBKBP1 and TBK1 form a growth factor signalling axis mediating immunosuppression and tumourigenesis. Nat. Cell Biol. *21*, 1604–1614. https://doi.org/10.1038/s41556-019-0429-8.

46. An, T., Li, S., Pan, W., Tien, P., Zhong, B., Shu, H.B., and Wu, S. (2015). DYRK2 negatively regulates Type I interferon induction by promoting TBK1 degradation via Ser527 phosphorylation. PLOS Pathog. *11*, e1005179. https://doi.org/10.1371/journal.ppat.1005179.

47. Hardie, D.G., and Ashford, M.L. (2014). AMPK: regulating energy balance at the cellular and whole body levels. Physiology (Bethesda) *29*, 99–107. https://doi.org/10.1152/physiol.00050.2013.

48. Hardie, D.G., Ross, F.A., and Hawley, S.A. (2012). AMPK: a nutrient and energy sensor that maintains energy homeostasis. Nat. Rev. Mol. Cell Biol. *13*, 251–262. https://doi.org/10.1038/nrm3311.

49. Lin, S.C., and Hardie, D.G. (2018). AMPK: sensing glucose as well as cellular energy status. Cell Metab. *27*, 299–313. https://doi.org/10.1016/j.cmet.2017.10.009.

50. Zhang, C.S., Jiang, B., Li, M., Zhu, M., Peng, Y., Zhang, Y.L., Wu, Y.Q., Li, T.Y., Liang, Y., Lu, Z., et al. (2014). The lysosomal v-ATPase-Ragulator complex is a common activator for AMPK and mTORC1, acting as a switch between catabolism and anabolism. Cell Metab. *20*, 526–540. https://doi.org/10.1016/j.cmet.2014.06.014.

51. Zhang, C.S., Hawley, S.A., Zong, Y., Li, M., Wang, Z., Gray, A., Ma, T., Cui, J., Feng, J.W., Zhu, M., et al. (2017). Fructose-1,6-bisphosphate and aldolase mediate glucose sensing by AMPK. Nature *548*, 112–116. https://doi.org/10.1038/nature23275.

52. Garcia, D., and Shaw, R.J. (2017). AMPK: mechanisms of cellular energy sensing and restoration of metabolic balance. Mol. Cell *66*, 789–800. https://doi.org/10.1016/j.molcel.2017.05.032.

53. González, A., Hall, M.N., Lin, S.C., and Hardie, D.G. (2020). AMPK and TOR: the yin and yang of cellular nutrient sensing and growth control. Cell Metab. *31*, 472–492. https://doi.org/10.1016/j.cmet.2020.01.015.

54. Mouchiroud, L., Eichner, L.J., Shaw, R.J., and Auwerx, J. (2014). Transcriptional coregulators: fine-tuning metabolism. Cell Metab. *20*, 26–40. https://doi.org/10.1016/j.cmet.2014.03.027.

55. Singhal, A., Jie, L., Kumar, P., Hong, G.S., Leow, M.K., Paleja, B., Tsenova, L., Kurepina, N., Chen, J., Zolezzi, F., et al. (2014). Metformin as adjunct antituberculosis therapy. Sci. Transl. Med. *6*, 263ra159. https://doi.org/10.1126/scitranslmed.3009885.

56. Moser, T.S., Schieffer, D., and Cherry, S. (2012). AMP-activated kinase restricts Rift Valley fever virus infection by inhibiting fatty acid synthesis. PLoS Pathog. *8*, e1002661. https://doi.org/10.1371/journal.ppat.1002661.

57. Mankouri, J., Tedbury, P.R., Gretton, S., Hughes, M.E., Griffin, S.D., Dallas, M.L., Green, K.A., Hardie, D.G., Peers, C., and Harris, M. (2010). Enhanced hepatitis C virus genome replication and lipid accumulation mediated by inhibition of AMP-activated protein kinase. Proc. Natl. Acad. Sci. USA *107*, 11549–11554. https://doi.org/10.1073/pnas.0912426107.

58. Blagih, J., Coulombe, F., Vincent, E.E., Dupuy, F., Galicia-Vázquez, G., Yurchenko, E., Raissi, T.C., van der Windt, G.J., Viollet, B., Pearce, E.L., et al. (2015). The energy sensor AMPK regulates T cell metabolic adaptation and effector responses in vivo. Immunity *42*, 41–54. https://doi.org/10.1016/j.immuni.2014.12.030.

59. Zhao, P., Wong, K.I., Sun, X., Reilly, S.M., Uhm, M., Liao, Z., Skorobogatko, Y., and Saltiel, A.R. (2018). TBK1 at the crossroads of inflammation and energy homeostasis in adipose tissue. Cell *172*, 731–743.e12. https://doi.org/10.1016/j.cell.2018.01.007.

60. Prantner, D., Perkins, D.J., and Vogel, S.N. (2017). AMP-activated kinase (AMPK) promotes innate immunity and antiviral defense through modulation of stimulator of interferon genes (STING) signaling. J. Biol. Chem. *292*, 292–304. M116.763268. https://doi.org/10.1074/jbc.M116.763268.

61. Jean, C.M., Honarmand, S., Louie, J.K., and Glaser, C.A. (2007). Risk factors for West Nile virus neuroinvasive disease, California, 2005. Emerg. Infect. Dis. *13*, 1918–1920. https://doi.org/10.3201/eid1312.061265.

62. Toniolo, A., Cassani, G., Puggioni, A., Rossi, A., Colombo, A., Onodera, T., and Ferrannini, E. (2019). The diabetes pandemic and associated infections: suggestions for clinical microbiology. Rev. Med. Microbiol. *30*, 1–17. https://doi.org/10.1097/MRM.0000000000000155.

63. van Crevel, R., van de Vijver, S., and Moore, D.A.J. (2017). The global diabetes epidemic: what does it mean for infectious diseases in tropical

countries? Lancet Diabetes Endocrinol. *5*, 457–468. https://doi.org/10.1016/S2213-8587(16)30081-X.

64. Sardu, C., D'Onofrio, N., Balestrieri, M.L., Barbieri, M., Rizzo, M.R., Messina, V., Maggi, P., Coppola, N., Paolisso, G., and Marfella, R. (2020). Outcomes in patients with hyperglycemia affected by Covid-19: can we do more on glycemic control? Diabetes Care *43*, 1408–1415. https://doi.org/10.2337/dc20-0723.
65. Zhu, L., She, Z.G., Cheng, X., Qin, J.J., Zhang, X.J., Cai, J., Lei, F., Wang, H., Xie, J., Wang, W., et al. (2020). Association of blood glucose control and outcomes in patients with COVID-19 and pre-existing type 2 diabetes. Cell Metab. *31*, 1068–1077.e3. https://doi.org/10.1016/j.cmet.2020.04.021.
66. Zhang, Y., Cui, Y., Shen, M., Zhang, J., Liu, B., Dai, M., Chen, L., Han, D., Fan, Y., Zeng, Y., et al. (2020). Association of diabetes mellitus with disease severity and prognosis in COVID-19: a retrospective cohort study. Diabetes Res. Clin. Pract. *165*, 108227. https://doi.org/10.1016/j.diabres.2020.108227.
67. Yang, J.K., Feng, Y., Yuan, M.Y., Yuan, S.Y., Fu, H.J., Wu, B.Y., Sun, G.Z., Yang, G.R., Zhang, X.L., Wang, L., et al. (2006). Plasma glucose levels and diabetes are independent predictors for mortality and morbidity in patients with SARS. Diabet. Med. *23*, 623–628. https://doi.org/10.1111/j.1464-5491.2006.01861.x.
68. Tan, Y., and Kagan, J.C. (2019). Innate immune signaling organelles display natural and programmable signaling flexibility. Cell *177*, 384–398.e11. https://doi.org/10.1016/j.cell.2019.01.039.
69. Everts, B., Amiel, E., Huang, S.C., Smith, A.M., Chang, C.H., Lam, W.Y., Redmann, V., Freitas, T.C., Blagih, J., van der Windt, G.J., et al. (2014). TLR-driven early glycolytic reprogramming via the kinases TBK1-IKKvarepsilon supports the anabolic demands of dendritic cell activation. Nat. Immunol. *15*, 323–332. https://doi.org/10.1038/ni.2833.
70. Wang, A., Huen, S.C., Luan, H.H., Yu, S., Zhang, C., Gallezot, J.D., Booth, C.J., and Medzhitov, R. (2016). Opposing effects of fasting metabolism on tissue tolerance in bacterial and viral inflammation. Cell *166*, 1512–1525.e12. https://doi.org/10.1016/j.cell.2016.07.026.
71. Corton, J.M., Gillespie, J.G., Hawley, S.A., and Hardie, D.G. (1995). 5-aminoimidazole-4-carboxamide ribonucleoside. A specific method for activating AMP-activated protein kinase in intact cells? Eur. J. Biochem. *229*, 558–565. https://doi.org/10.1111/j.1432-1033.1995.tb20498.x.
72. Konagaya, Y., Terai, K., Hirao, Y., Takakura, K., Imajo, M., Kamioka, Y., Sasaoka, N., Kakizuka, A., Sumiyama, K., Asano, T., and Matsuda, M. (2017). A highly sensitive FRET biosensor for AMPK exhibits heterogeneous AMPK responses among cells and organs. Cell Rep. *21*, 2628–2638. https://doi.org/10.1016/j.celrep.2017.10.113.
73. Pinkosky, S.L., Scott, J.W., Desjardins, E.M., Smith, B.K., Day, E.A., Ford, R.J., Langendorf, C.G., Ling, N.X.Y., Nero, T.L., Loh, K., et al. (2020). Long-chain fatty acyl-CoA esters regulate metabolism via allosteric control of AMPK F0621 isoforms. Nat. Metab. *2*, 873–881. https://doi.org/10.1038/s42255-020-0245-2.
74. Cool, B., Zinker, B., Chiou, W., Kifle, L., Cao, N., Perham, M., Dickinson, R., Adler, A., Gagne, G., Iyengar, R., et al. (2006). Identification and characterization of a small molecule AMPK activator that treats key components of type 2 diabetes and the metabolic syndrome. Cell Metab. *3*, 403–416. https://doi.org/10.1016/j.cmet.2006.05.005.
75. Meng, F., Zhou, R., Wu, S., Zhang, Q., Jin, Q., Zhou, Y., Plouffe, S.W., Liu, S., Song, H., Xia, Z., et al. (2016). Mst1 shuts off cytosolic antiviral defense through IRF3 phosphorylation. Genes Dev. *30*, 1086–1100. https://doi.org/10.1101/gad.277533.116.
76. Xiang, W., Zhang, Q., Lin, X., Wu, S., Zhou, Y., Meng, F., Fan, Y., Shen, T., Xiao, M., Xia, Z., et al. (2016). PPM1A silences cytosolic RNA sensing and antiviral defense through direct dephosphorylation of MAVS and TBK1. Sci. Adv. *2*, e1501889. https://doi.org/10.1126/sciadv.1501889.
77. Hardie, D.G., Schaffer, B.E., and Brunet, A. (2016). AMPK: an energy-sensing pathway with multiple inputs and outputs. Trends Cell Biol. *26*, 190–201. https://doi.org/10.1016/j.tcb.2015.10.013.
78. Schaffer, B.E., Levin, R.S., Hertz, N.T., Maures, T.J., Schoof, M.L., Hollstein, P.E., Benayoun, B.A., Banko, M.R., Shaw, R.J., Shokat, K.M., and Brunet, A. (2015). Identification of AMPK phosphorylation sites reveals a network of proteins involved in cell invasion and facilitates large-scale substrate prediction. Cell Metab. *22*, 907–921. https://doi.org/10.1016/j.cmet.2015.09.009.
79. Gwinn, D.M., Shackelford, D.B., Egan, D.F., Mihaylova, M.M., Mery, A., Vasquez, D.S., Turk, B.E., and Shaw, R.J. (2008). AMPK phosphorylation of raptor mediates a metabolic checkpoint. Mol. Cell *30*, 214–226. https://doi.org/10.1016/j.molcel.2008.03.003.
80. Lai, Y.C., Kviklyte, S., Vertommen, D., Lantier, L., Foretz, M., Viollet, B., Hallén, S., and Rider, M.H. (2014). A small-molecule benzimidazole derivative that potently activates AMPK to increase glucose transport in skeletal muscle: comparison with effects of contraction and other AMPK activators. Biochem. J. *460*, 363–375. https://doi.org/10.1042/BJ20131673.
81. Ma, T., Tian, X., Zhang, B., Li, M., Wang, Y., Yang, C., Wu, J., Wei, X., Qu, Q., Yu, Y., et al. (2022). Low-dose metformin targets the lysosomal AMPK pathway through PEN2. Nature *603*, 159–165. https://doi.org/10.1038/s41586-022-04431-8.
82. Jaishankar, D., Yakoub, A.M., Yadavalli, T., Agelidis, A., Thakkar, N., Hadigal, S., Ames, J., and Shukla, D. (2018). An off-target effect of BX795 blocks herpes simplex virus type 1 infection of the eye. Sci. Transl. Med. *10*. https://doi.org/10.1126/scitranslmed.aan5861.
83. Crampton, S.P., and Bolland, S. (2013). Spontaneous activation of RNA-sensing pathways in autoimmune disease. Curr. Opin. Immunol. *25*, 712–719.
84. Gao, D., Li, T., Li, X.D., Chen, X., Li, Q.Z., Wight-Carter, M., and Chen, Z.J. (2015). Activation of cyclic GMP-AMP synthase by self-DNA causes autoimmune diseases. Proc. Natl. Acad. Sci. USA *112*, E5699–E5705. https://doi.org/10.1073/pnas.1516465112.
85. Ishikawa, H., Ma, Z., and Barber, G.N. (2009). STING regulates intracellular DNA-mediated, type I interferon-dependent innate immunity. Nature *461*, 788–792. nature08476. https://doi.org/10.1038/nature08476.
86. Shang, G., Zhang, C., Chen, Z.J., Bai, X.C., and Zhang, X. (2019). Cryo-EM structures of STING reveal its mechanism of activation by cyclic GMP-AMP. Nature *567*, 389–393. https://doi.org/10.1038/s41586-019-0998-5.
87. Zhao, B., Du, F., Xu, P., Shu, C., Sankaran, B., Bell, S.L., Liu, M., Lei, Y., Gao, X., Fu, X., et al. (2019). A conserved PLPLRT/SD motif of STING mediates the recruitment and activation of TBK1. Nature *569*, 718–722. https://doi.org/10.1038/s41586-019-1228-x.
88. Hasan, M., Gonugunta, V.K., Dobbs, N., Ali, A., Palchik, G., Calvaruso, M.A., DeBerardinis, R.J., and Yan, N. (2017). Chronic innate immune activation of TBK1 suppresses mTORC1 activity and dysregulates cellular metabolism. Proc. Natl. Acad. Sci. USA *114*, 746–751. https://doi.org/10.1073/pnas.1611113114.
89. Ran, F.A., Hsu, P.D., Wright, J., Agarwala, V., Scott, D.A., and Zhang, F. (2013). Genome engineering using the CRISPR-Cas9 system. Nat. Protoc. *8*, 2281–2308. https://doi.org/10.1038/nprot.2013.143.
90. Zhao, Y., Zhao, J., Zhao, C., Zhou, H., Li, Y., Zhang, J., Li, L., Hu, C., Li, W., Peng, X., et al. (2015). A metabolomics study delineating geographical location-associated primary metabolic changes in the leaves of growing tobacco plants by GC-MS and CE-MS. Sci. Rep. *5*, 16346. https://doi.org/10.1038/srep16346.

Please cite this article in press as: Zhang et al., AMPK directly phosphorylates TBK1 to integrate glucose sensing into innate immunity, Molecular Cell (2022), https://doi.org/10.1016/j.molcel.2022.10.026

STAR★METHODS

KEY RESOURCES TABLE

REAGENT or RESOURCE	SOURCE	IDENTIFIER
Antibodies		
Rabbit monoclonal anti-IRF3	Cell Signaling Technology	Cat#4302; RRID: AB_1904036
Rabbit monoclonal anti-IRF3	Abcam	Cat#ab68481; RRID: AB_11155653
Rabbit monoclonal anti-IRF3 (phospho S396)	Cell Signaling Technology	Cat#4947; RRID: AB_823547
Rabbit monoclonal anti-IRF3 (phospho S386)	Abcam	Cat#ab76493; RRID: AB_1523836
Rabbit monoclonal anti-TBK1/NAK	Cell Signaling Technology	Cat#3504; RRID: AB_2255663
Rabbit monoclonal anti-TBK1/NAK (phospho S172)	Cell Signaling Technology	Cat#5483; RRID: AB_10693472
Rabbit monoclonal anti-AMPKα	Cell Signaling Technology	Cat#5831; RRID: AB_10622186
Rabbit monoclonal anti- AMPKα (phospho T172)	Cell Signaling Technology	Cat#50081; RRID: AB_2799368
Rabbit monoclonal anti-ACC	Cell Signaling Technology	Cat#3676; RRID: AB_2219397
Rabbit monoclonal anti-ACC (phospho S79)	Cell Signaling Technology	Cat#3661; RRID: AB_330337
Rabbit monoclonal anti-ULK1	Cell Signaling Technology	Cat#8054; RRID: AB_11178668
Rabbit monoclonal anti-ULK1 (phospho S555)	Cell Signaling Technology	Cat#5869; RRID: AB_10707365
Rabbit monoclonal anti-Raptor	Cell Signaling Technology	Cat#2280; RRID: AB_561245
Rabbit monoclonal anti- Raptor (phospho S792)	Cell Signaling Technology	Cat#2083; RRID: AB_2249475
Rabbit monoclonal anti-S6K	Cell Signaling Technology	Cat#2708; RRID: AB_390722
Rabbit monoclonal anti- S6K (phospho T389)	Cell Signaling Technology	Cat#97596; RRID: AB_2800283
Rabbit monoclonal anti-Atg13	Cell Signaling Technology	Cat#13273; RRID: AB_2798169
Rabbit monoclonal anti- Atg13 (phospho S355)	Cell Signaling Technology	Cat#46329; RRID: AB_2313773
Rabbit monoclonal anti-FIP200	Cell Signaling Technology	Cat#12436; RRID: AB_2797913
Rabbit monoclonal anti-STAT1	Cell Signaling Technology	Cat#14994; RRID: AB_2737027
Rabbit monoclonal anti- STAT1 (phospho S727)	Cell Signaling Technology	Cat#8826; RRID: AB_2773718
Mouse monoclonal anti-Myc Tag	Cell Signaling Technology	Cat#3739, RRID: AB_10889248
Rabbit monoclonal anti-HA Tag	Cell Signaling Technology	Cat#3724; RRID: AB_1549585
Rabbit monoclonal anti-RIG-I	Cell Signaling Technology	Cat#3743; RRID: AB_2269233
Mouse monoclonal anti-α-Tubulin (clone DM1A)	Sigma-Aldrich	Cat#T6199; RRID: AB_477583
Anti-Flag affinity gel	Sigma-Aldrich	Cat#F3165; RRID: AB_259529
Mouse monoclonal anti-HA Tag	Sigma-Aldrich	Cat#H9658; RRID: AB_260092
Mouse monoclonal anti-β-actin	Sigma-Aldrich	Cat#A5441; RRID: AB_476744
Rabbit monoclonal anti-STING	Abcam	Cat#ab181125; RRID:AB_2916053
Rabbit monoclonal anti-GM130	BD Bioscience	Cat#610822; RRID:AB_398141
Rabbit polyclonal anti-TBK1 (phospho S511)	This paper	N/A
Bacterial and virus strains		
GFP-tagged Vesicular Stomatitis Virus (VSV)	Zhijian J. Chen	N/A
Sendai Virus (SeV)	Charles River laboratories	Cat#VR-907
Mammalian Orthoreovirus (MRV)	Yaowei Huang	N/A
Swine Acute Diarrhea Syndrome Coronavirus (SADS-CoV)	Yaowei Huang	N/A
GFP tagged recombination adenovirus Ad5-GFP	Yaowei Huang	N/A
Herpes Simplex Virus-1 (HSV-1)	Zhengfan Jiang	N/A
GFP and Luciferase double-tagged Herpes Simplex Virus-1 (HSV-1)	Jiahuai Han	N/A

(*Continued on next page*)

Please cite this article in press as: Zhang et al., AMPK directly phosphorylates TBK1 to integrate glucose sensing into innate immunity, Molecular Cell (2022), https://doi.org/10.1016/j.molcel.2022.10.026

Continued

REAGENT or RESOURCE	SOURCE	IDENTIFIER
Chemicals, peptides, and recombinant proteins		
Poly (I:C) LMW	Invivogen	Cat#tlrl-picw
cGAMP	Invivogen	Cat#tlrl-nacga23-02
poly (dA:dT)	Invivogen	Cat#tlrl-patn
Lipofectamine RNAiMAX	Invitrogen	Cat#13778-150
Rapamycin	Selleck	S1039; CAS: 53123-88-9
SBI-0206965	Selleck	S7885; CAS: 1884220-36-3
Compound C	Selleck	S7306; CAS: 1219168-18-9
AICAR	Selleck	S7885; CAS: 1884220-36-3
991	Selleck	S8654; CAS: 1219739-36-2
MRT68921	Selleck	S7949; CAS: 2070014-87-6
A-769662	Selleck	S2697; CAS: 844499-71-4
ABT-737	Selleck	S1002; CAS: 852808-04-9
qVD-OPH	Selleck	S7311; CAS: 1135695-98-5
S63845	Selleck	S8383; CAS: 1799633-27-4
MK2206	Selleck	S1078; CAS: 1032350-13-2
2-DG	Sangon Biotech	A602241; CAS: 154-17-6
Doxycycline hydrochloride	Sangon Biotech	A600889; CAS: 24390-14-5
Hydroxyurea (HU)	Sigma-Aldrich	H8627; CAS: 127-07-1
Metformin	Sigma-Aldrich	PHR1084; CAS: 1115-70-4
D-(+)-Glucose	Sigma-Aldrich	G5146; CAS: 50-99-7
Puromycin Dihydrochloride	Yeasen	60210ES25; CAS: 58-58-2
G418 Sulfate(Geneticin)	Yeasen	60220ES03; CAS: 108321-42-2
Critical commercial assays		
QuikChange Site-Directed Mutagenesis Kit	Stratagene	Cat#200519
Q5® High-Fidelity 2X Master Mix	NEW ENGLAND BioLabs	Cat#M0492L
KOD Hot Start DNA Polymerase	Merck Milipore	Cat#71086
Dual-Luciferase Reporter Assay System	Promega	Cat#E1910
AxyPrep Multisource Total RNA Miniprep Kit	Axygen	Cat#AP-MN-MS-RNA-50
All-in-One cDNA Synthesis SuperMix	Bimake	Cat#24408
EvaGreen qPCR MasterMix	Abm	Cat#MasterMix-R
Deposited data		
The mass spectrometry proteomics data of TBK1 modifications by AMPKα1	This paper	PXD033926
Original data in Mendeley Data	This paper	https://doi.org/10.17632/mp29sk7v29.2
Experimental models: Cell lines		
HEK293T	ATCC	Cat#CRL-3216
HCT116	ATCC	Cat#CCL-247
DLD1	ATCC	Cat#CCL-221
MEFs	ATCC	Cat#CF-1
Peritoneal Macrophages	This paper	N/A
Intestinal organoids	This paper	N/A
Experimental models: Organisms/strains		
Mouse: TBK1$^{S511E/S511E}$ C57BL/6 knock-in mice	GemPharmatech	N/A
Mouse: Dnm1l$^{S511A/S511A}$ C57BL/6 knock-in mice	GemPharmatech	N/A
Mouse: AMPKAR-EV mice	From Dr. Michiyuki Matsuda	N/A
Mouse: AMPKα1/α2^{Flox}+ Lyz^{Cre} mice	From Dr. Shengcai Lin	N/A
Zebrafish: zebrafish AB wild-type	From Dr. Jian Zou	N/A

(*Continued on next page*)

Please cite this article in press as: Zhang et al., AMPK directly phosphorylates TBK1 to integrate glucose sensing into innate immunity, Molecular Cell (2022), https://doi.org/10.1016/j.molcel.2022.10.026

Continued

REAGENT or RESOURCE	SOURCE	IDENTIFIER
Mouse: C57BL/6 mice wild-type	SLAC Laboratory Animal	N/A
Mouse: BALB/c mice wild-type	SLAC Laboratory Animal	N/A
Oligonucleotides		
See Table S1 for the List of Oligos for RT-qPCR and sgRNA	This paper	N/A
Recombinant DNA		
See Table S2 for the List of Recombinant DNA	This paper	N/A
Software and algorithms		
GraphPad Prism 8.0	GraphPad	https://www.graphpad.com/scientific-software/prism/
Origin 9.0	OriginLab	https://www.originlab.com/index.aspx?go=PRODUCTS/Origin
Image-Pro Plus 6.0	Media Cybernetics	https://www.mediacy.com/imageproplus
ImageJ	ImageJ	https://imagej.nih.gov/ij/

RESOURCE AVAILABILITY

Lead contact

Further information and requests for resources and reagents should be directed to and will be fulfilled by the Lead Contact, Pinglong Xu (xupl@zju.edu.cn).

Materials availability

Pinglong Xu is responsible for all reagent and resource requests. Please contact Pinglong Xu (xupl@zju.edu.cn) with requests and inquiries.

Data and code availability

The mass spectrometry proteomics data have been deposited at ProteomeXchange Consortium (http://proteomecentral.proteomexchange.org) via the iProX partner repository[1] with the dataset identifier PXD033926 and are publicly available as of the date of publication. Accession number is listed in the key resources table. Original data of western blot images and statistics source data of the manuscript have been deposited at Mendeley data (https://doi.org/10.17632/mp29sk7v29.2) and are publicly available as of the date of publication. Microscopy data reported in this paper will be shared by the lead contact upon request.

No original code has been generated in this study.

Any additional information required to reanalyze the data reported in this paper is available from the lead contact upon request.

EXPERIMENTAL MODEL AND SUBJECT DETAILS

Mice

TBK1 S511E and TBK1 S511A transgenic mice were on C57BL/6 background, and both male and female littermates were used in all the experiments. GemPharmatech generated TBK1 Knock-in transgenic C57BL/6 mice. To create point mutations (S511E, S511A) at mouse Tbk1 locus by CRISPR/Cas9-mediated genome engineering,[89] Tbk1 S511E (TCT to GAA), and Tbk1 S511A (TCT to GCC) specific sgRNA oligos were designed by the CRISPR website (http://crispr.mit.edu/) targeting sequence at S511 locus (5'- TTCTAT TGTTCCCTGAGAAC -3') and (5'- ATTTAGCTTTCCAGTTCTCA -3'), with S511E oligo donor sequence (5'- CATTTGG ATCTGATCCGTTGTTCTGACCTAACCTAACCCGTTGTATTTAGCTTTCCAGCGAACAGGGAACAATAGAAAGCAGTCTTCAGGACA TCAGCAGCAGGCTGTCTCCAGGGGGCT -3') and S511A oligo donor sequence (5'- CATTTGGATCTGATCCGTTGTTCTGACC TAACCTA ACCCGTTGTATTTAGCTTTCCAGCGCCCAGGGAACAATAGAAAGCAGTCTTCAGGACATCAGCAGCAGGCTGTCTCC AGGGGGCT -3'). Cas9 mRNA and sgRNA generated by in vitro transcription and donor oligo were co-injected into fertilized eggs for knock-in mouse production. The target region of the mouse Tbk1 locus was sequenced to confirm targeting. The AMPKAR-EV transgenic mice, in which real-time AMPK activity can be observed via *in vivo* imaging with two-photon excitation microscopy, were described previously.[72] The AMPKα1/α2^{Flox}+ Lyz^{Cre} mice, in which the AMPKα1/α2 subunits were double knockout in a myeloid line, were obtained by crossing the AMPKα1/α2^{Flox} mice[50] with the Lyz^{Cre} line.

Male 6-8 weeks old wild-type BALB/c mice and LVG hamsters were purchased from SLAC Laboratory Animal for the murine virus infection. Zebrafish AB wild-type embryos (male/female) were raised at 28.5°C in E3 egg water.

All the animals were bred and maintained in a pathogen-free animal facility at the laboratory animal center of Zhejiang University. The care of experimental animals was approved by the Zhejiang University committee and followed Zhejiang University guidelines.

Zebrafish

Zebrafish AB wild-type embryos (male/female) were raised at 28.5°C in E3 egg water. The care of experimental animals was approved by the Zhejiang University committee and followed Zhejiang University guidelines.

Peritoneal Macrophages

Peritoneal macrophages were isolated from C57BL/6 mice at 6-8 weeks of age with the Brewer thioglycollate medium (Sigma-Aldrich)-induced approach. Three days after intraperitoneal injection of 2.5 mL of 3% thioglycollate medium, peritoneal macrophages were isolated and cultured in RPMI 1640 medium.

Cell Lines

HEK293, HCT116, DLD1, and MEFs cells were from ATCC. No cell lines used in this study were found in the database of commonly misidentified cell lines maintained by ICLAC and NCBI Biosample. Cell lines were frequently checked in morphology under microscopy and tested for mycoplasma contamination but were not authenticated. All cell lines, except for peritoneal macrophages that were maintained in RPMI 1640 medium, were cultured in DMEM medium with 10% fetal bovine serum (FBS) at 37°C in 5% CO_2 (v/v).

The TBK1 inducible expressing DLD1 cells were generated by the lentiviral vector infection containing an inducible Tet-On system (Sigma) followed by the open read frame (ORF) of TBK1 and selected by G418 antibiotic at a concentration of 1500 μg mL^{-1} for one week. DLD1 cells and MEFs with stable expressing AMPKα1 were generated with the lentiviral vector pBobi followed by the ORF of AMPKα1 and selected by puromycin at a concentration of 1 μg ml^{-1} for three days.

Intestinal Organoids

Isolated small intestines were opened longitudinally, washed three times with cold PBS, removed the villi by scraping, and incubated twice in cold PBS with 2 mM EDTA for 15 min on ice. After removing the EDTA medium, the fractions were incubated in 50 mL cold PBS with a fierce shake and passed through a 70-μm cell strainer (BD Bioscience) to remove the residual villous material. Isolated crypts were centrifuged at 300 g for 5 min to separate the crypts with single cells. The centrifuged fractions were suspended and cultured in Matrigel with medium (Advanced DMEM/F12 supplemented with penicillin/streptomycin, 10 mM HEPES, Glutamax, 13N2, 13B27 (all from Invitrogen), and 1mM N-acetylcysteine (Sigma) containing growth factors 50 ng mL^{-1} EGF, 100 ng mL^{-1} noggin, 1mg mL^{-1} R-spondin). The organoid formation was observed and analyzed every day after plating.

Viruses

SeV was produced by inoculating the virus into the chorioallantoic sac of 9 to 11-day-old embryonated SPF chicken eggs. High titer stocks of VSV, HSV-1, MRV, Ad5-GFP, and SADS-CoV were produced in BHK-21 cells by using seed stocks. All the viruses were stocked at -80°C.

METHOD DETAILS

Expression Plasmids, Viruses, Reagents, and Antibodies

Expression plasmids encoding Flag-, Myc-, or HA-tagged wild-type or mutations, or the truncations of human MAVS, STING, caRIG-I, TBK1, IKKε, IRF3, K48-Ub, and the reporters of IFNβ_Luc and 5xISRE_Luc have been described previously.[40,42] ORFs of AMPKα1, AMPKα2, AMPKβ2, AMPKγ2, AMPKγ3, ULK1 and AKT1 were obtained from Invitrogen ORF Lite Clone Collection cDNA library by PCR, and Flag- or HA-tagged human AMPKα1, AMPKα2, ULK1 and AKT1 were constructed using the pRK5 mammalian expression vector. Truncations of AMPKα1, including a.a. 1-280, 281-559, 1-385, 386-559, and site-directed mutagenesis about TBK1 S511A/D/E, TBK1 S510A/D, and AMPKα1 T172D were generated by PCR-based cloning performed by a kit from Stratagene. All coding sequences were verified by DNA sequencing, and the detailed information for construction was provided in the attached Table S2 and upon requirement.

The GFP and Luciferase double-tagged HSV-1 was gifted from Dr. Jiahuai Han (Xiamen University, Xiamen), GFP-tagged HSV-1 was gifted from Dr. Zhengfan Jiang (Beijing University, Beijing), GFP-tagged VSV was gifted from Dr. Zhijian J. Chen (UT Southwestern Medical Center, Dallas), and Sendai virus (Cantell strain) was from Charles River Laboratories. Mammalian orthoreovirus MRV, SADS-CoV, and GFP tagged recombination adenovirus Ad5-GFP was by the laboratory of Dr. Yao-Wei Huang (Zhejiang University, Hangzhou). The pharmacological reagents Rapamycin (Selleck), SBI-0206965 (Selleck), Compound C (Selleck), AICAR (Selleck), 991 (Selleck), MRT68921 (Selleck), A-769662 (Selleck), ABT-737 (Selleck), qVD-OPH (Selleck), S63845 (Selleck), MK2206 (Selleck), Doxycycline (Sangon Biotech), 2-DG (Sangon Biotech), cGAMP (Invivogen), poly(I:C) (Invivogen), poly (dA:dT) (Invivogen), puromycin (Yeasen), G418 (Yeasen), Hydroxyurea (HU) (Sigma), and Metformin (Sigma) were purchased and used according to manual instructions.

The monoclonal anti-TBK1 (3504S, 1:5,000 dilution), anti-pTBK1(S172) (5483S, 1:3,000 dilution), anti-IRF3 (4302S, 1:2,000 dilution), anti-pIRF3 (S396) (4947S, 1:5,000 dilution), anti-pSTAT1 (S727) (8826, 1:1,000 dilution), anti-STAT1 (14994, 1:1,000 dilution),

anti-AMPKα (5831S, 1:1,000 dilution), anti-pAMPKα (T172) (50081S, 1:1,000 dilution), anti-S6K (2708S, 1:1,000 dilution), anti-pS6K (T389) (97596S, 1:1,000 dilution), anti-pULK1 (S555) (5869S, 1:1,000 dilution), anti-ULK1 (8054, 1:1,000 dilution), anti-pACC (S79) (3661S, 1:1,000 dilution), anti-ACC (3676S, 1:1,000 dilution), anti-pRaptor (S792) (2083, 1:1,000 dilution), anti-Raptor (2280, 1:1,000 dilution), anti-pAtg13 (S355) (46329, 1:1,000 dilution), anti-Atg13 (13273, 1:1,000 dilution), anti-FIP200 (12436, 1:1,000 dilution), anti-RIG-I (3743S, 1:1,000 dilution), anti-Myc (2276S, 1:3,000 dilution), and anti-HA (3724S, 1:5,000 dilution) antibodies were purchased from Cell Signaling Technology. The anti-pIRF3 (S386) (ab76493, 1:3,000 dilution), anti-STING (ab181125, 1:100 dilution) were purchased from Abcam, and the anti-α-tubulin (T6199, 1:10,000 dilution), anti-β-actin (A5441, 1:10,000 dilution), anti-HA (H9658, 1:200 dilution), and anti-Flag (M2) (F3165, 1:5,000 dilution) were purchased from Sigma. The anti-GM130 (610822, 1:2,000 dilution) was purchased from BD Bioscience. The anti-rabbit IgG, and anti-mouse IgG antibodies were purchased from Santa Cruz. The anti-pTBK1 (S511) was generated in collaboration with Abcam, targeting the phospho-TBK1 S511.

Plasmids Transfection and Virus Infection of Cultured Cells

Lipofectamine 3000 (Invitrogen), Polyethyleneimine (PEI, Polysciences), or Lipofectamine RNAiMAX (Invitrogen) transfection reagents were used for the transfection of plasmids, poly(dA:dT), and poly(I:C). Digitonin (Sigma) was used for cGAMP inducing.

The infection of SeV, VSV, Ad5-GFP or HSV-1 was as previously described.[75,76] Briefly, viruses with the indicated amount (0.5 - 5 moi) were added into the fresh and serum-free medium, and cells were incubated at 37°C in 5% CO_2 (v/v) for 1 hour, shaking mildly every 15 minutes. The virus-containing medium was replaced by a fresh medium containing 10% FBS.

CRISPR/Cas9-mediated Generation of AMPKα1/α2$^{-/-}$, ULK1/2$^{-/-}$, FIP200$^{-/-}$ and TBK1 Knock-in Cells

Guide RNA sequences targeting AMPKα1 and α2 mRNA sequence (hAMPKα1, 5'- AAAGTTTGAGTGCTCAGAAG -3', 5'- GTGATGGAATATGTCTCAGG -3'; hAMPKα2, 5'- TCAATTAACAGGCCATAAAG -3', 5'- GTTATTTAAGAAGATCCGAG -3'), ULK1 and ULK2 mRNA sequence (hULK1, 5'- GGTCTTCGGGAAGTCAAAGG -3', hULK2, 5'- GTAAGGCCTAGAAGACCCAG -3'), FIP200 mRNA sequence (hFIP200, 5'- AGGAGAGAGCACCAGTTCAG -3'), TBK1 S511A/D knock-in mRNA sequence (hTBK1, 5'- TATTTAGCTTTCCAGTTCTC -3', 5'- TTCTATTGTTCCCTGAGAAC -3') were used to clone the genes into the vector pgRNA, which were transfected into DLD1 cells by LipofectAmine 3000, together with the pCas9-2A-GFP plasmid, or with pCas9-2A-GFP and pMD18 in the case of TBK1 S511A/D knock-in generation.[89] Thirty-six hours after transfection, cells with green fluorescence were sorted with a Flow Cytometer (BD FACS Aria II) and propagated. Clones were identified by immunoblotting with anti-AMPKα or the sequencing of the genomic PCR products. All gRNAs used in the experiments were also attached in Table S1.

Luciferase Reporter Assay

HEK293 cells were transfected with indicated reporters (100 ng) bearing an open read frame (ORF) coding Firefly luciferase, along with the pRL-Luc with Renilla luciferase coding as the internal control for transfection and other expression vectors specified in the results section. In brief, after 24 hours post-transfection, cells were lysed by passive lysis buffer (Promega), and luciferase assays were performed using a dual luciferase assay kit (Promega), quantified with POLARstar Omega (BMG Labtech), and normalized to the internal Renilla luciferase control.

Quantitative RT-PCR Assay

The PMs, DLD1, HCT116 cells, and intestinal organoid stimulated with cGAMP, AQS, poly (I:C), VSV, SeV, HSV-1, and Hydroxyurea (HU) were lysed, and total RNA was extracted using an RNAeasy extraction kit (Axygen). cDNA was generated by a one-step iScript cDNA synthesis kit (Vazyme), and quantitative real-time PCR was performed using the EvaGreen Qpcr MasterMix (Abm) and CFX96 real-time PCR system (Bio-Rad). Relative quantification was expressed as $2^{-\Delta Ct}$, where C_t is the difference between the primary C_t value of triplicates of the sample and an endogenous L19 or GAPDH mRNA control. The human, mouse or zebrafish primer sequences used are listed in the following:

hIFIT1, 5'- TTGATGACGATGAAATGCCTGA -3', 5'- CAGGTCACCAGACTCCTCAC -3'; hIFIT2, 5'- GACACGGTTAAAGTGT GGAGG -3', 5'- TCCAGACGGTAGCTTGCTATT -3'; hCXCL10, 5'- GTGGCATTCAAGGAGTACCTC -3', 5'- TGATGGCCTTC GATTCTGGATT -3'; hIFNB1, 5'- ATGACCAACAAGTGTCTCCTCC -3', 5'- GGAATCCAAGCAAGTTGTAGCTC-3'; hISG15, 5'- CGCAGATCACCCAGAAGATCG -3', 5'- TTCGTCGCATTTGTCCACCA -3'; mIFNB1, 5'- CAGCTCCAAGAAAGGACGAAC -3', 5'- GGCAGTGTAACTCTTCTGCAT -3'; mIRF7, 5'- GAGACTGGCTATTGGGGGAG -3', 5'- GACCGAAATGCTTCCAGGG -3'; mIFIT1, 5'- CTGAGATGTCACTTCACATGGAA -3', 5'- GTGCATCCCCAATGGGTTCT -3'; mIFIT2, 5'- AGTACAACGAGTAAGGA GTCACT -3', 5'- AGGCCAGTATGTTGCACATGG -3'; mISG15, 5'- GGTGTCCGTGACTAACTCCAT -3', 5'- TGGAAAGGGTAA GACCGTCCT -3'; mTNFα, 5'- CCCTCACACTCAGATCATCTTCT -3', 5'- GCTACGACGTGGGCTACAG -3'; IFNphi1, 5'- CTGCAGAG TCAAAGCTCTGCGTCTAC -3', 5'- CTTGTCCATCAAGGTGTACAAGCGG -3'; IFNphi4, 5'- GACAATGAGGACCTCAACCCCATCC -3', 5'- GGGAACAAGTGCATCGTCGAAGAGG -3'; zebrafish IRF7, 5'- GTACGAGGGTTTGAGCATGATAGGC -3', 5'- GTTGATCTT GCCGCTGACTATAGCC -3', RPL19, 5'-ATGTATCACAGCCTGTACCTG -3', 5'- TTCTTGGTCTCTTCCTCCTTG -3'; HSV-1, 5'- GGCCTGGCTATCCGGAGA -3', 5'- GCGCAGAGACATCGCGA -3', VSV, 5'- ACGGCGTACTTCCAGATGG -3', 5'- CTCGGTTC AAGATCCAGGT -3'. All primers used in the qRT-PCR assay were also attached in Table S1.

Please cite this article in press as: Zhang et al., AMPK directly phosphorylates TBK1 to integrate glucose sensing into innate immunity, Molecular Cell (2022), https://doi.org/10.1016/j.molcel.2022.10.026

Coimmunoprecipitations and Immunoblottings

HEK293, PMs, MEF, HCT116, or DLD1 cells were stimulated with cGAMP, poly (I:C), and poly (dA:dT), infected with VSV, HSV-1, and SeV, or transfected with specified plasmids encoding Myc-, Flag-, or HA-tagged AMPKα1, AMPKα2, caRIG-I, MAVS, TBK1s, IKKε, IRF3s, and STING was lysed using the modified MLB lysis buffer (20 mM Tris-Cl, 200 mM NaCl, 10 mM NaF, 1 mM NaV_2O_4, 1% NP-40, 20 mM β-glycerophosphate, and protease inhibitor, pH 7.5).[32] Cell lysates were then subjected to immunoprecipitation using the antibodies of anti-Flag (Sigma, F3165-5MG, 1:200 dilution), anti-Myc (CST, 2276S, 1:200 dilution), or anti-HA (Sigma, H9658, 1:200 dilution) for transfected or induced proteins. After 3-4 washes with the MLB, adsorbed proteins were resolved by SDS-PAGE (Bio-Rad) and immunoblotting with the indicated antibodies. Cell lysates were also analyzed using SDS-PAGE and immunoblotting to control the protein abundance.

In vitro Kinase Assay

HEK293 cells were transfected with plasmids encoding Flag-, Myc-, or HA-tagged TBK1s or AMPKα and lysed by the modified MLB lysis buffer after 24 hours of transfection. Immunoprecipitations were performed by using with anti-Flag (Sigma, F3165-5MG, 1:200 dilution), anti-Myc (2276S, 1:200 dilution), or anti-HA (CST, 3724S, 1:200 dilution) antibodies. With two washes by the MLB and two washes by the kinase assay buffer (200 μM ATP, 200 μM AMP, 20 mM Tris-HCl, 1 mM EGTA, 5 mM $MgCl_2$, 0.02% 2-mercapto-Ethanol, 0.03% Brij-35, and 0.2 mg mL^{-1} BSA, PH 7.4), immunoprecipitated TBK1s and AMPKα1 were incubated in the kinase assay buffer at 30°C for 60 min on THERMO-SHAKER (1400 rpm/min), in the presence of 20 μM ATP (Abcam). The reaction was stopped by adding 2 × SDS loading buffer and subjected to SDS-PAGE and specified immunoblotting.

Immunofluorescence, Microscopy, and FACS

DLD1 cells were treated with cGAMP for 2-4 hours before harvest, fixed in 4% paraformaldehyde, blocked in 10% horse serum in PBS for 2 hours, and incubated sequentially with primary antibodies anti-GM130 (BD, 610822, 1:2000 dilution) or anti-STING (Abcam, ab181125, 1:200 dilution) and Alexa-labeled secondary antibodies (Jackson, 111-095-003; 115-095-003; 111-025-003; 115-025-003, 1:500 dilution) with extensive washing. Slides were stained with DAPI (Santa Cruz Biotech) and mounted with ProLong™ Gold antifade reagent (Invitrogen). Immunofluorescence images were obtained and analyzed using the Nikon Eclipse Ti inverted microscope or the Zeiss LSM710 confocal microscope. FACS analyses of GFP^+ cells were performed at BD FACSCalibur or Beckman CytoFlex, according to the manufacturer's manual.

VSV Challenge in Zebrafish

Zebrafish embryos were microinjected with gVSV virus (1×10^3 pfu per embryo) in the yolk at 48 hours post-fertilization (hpf) and treated with or without AICAR (500 μM) or Compound C (10 μM). The infection and death ratio of injected embryos were recorded at the desired stages, and infection was confirmed by GFP expression that was integrated into the viral genome. In a parallel experiment, the desired tissue samples were homogenized after 24 hpi and subjected to RNA extraction and qRT-PCR assays to detect cytokines' expression, including IFNφ1, IFNφ4, and IRF7. Meanwhile, the desired tissue samples were homogenized and lysed in the MLB to detect the activation of AMPK by immunoblotting.

Blood Glucose Level Measurement and Viral Challenge in Mice

To measure the survival of mice with viral challenges and upon the addition of D-(+)-glucose (Sigma-Aldrich G5146), eight-week-old C57BL/6 wild-type mice were tail intravenously injected with gVSV by a dose of 2×10^7 pfu per gram of animal weight and were per os (P.O.) gavage three times with saline (mock) or glucose (6 g/kg) every 6 hours, starting at 0 hpi. At 12 hpi, mice were supplemented with drinking water containing 20% glucose. For the food gavage experiment, as specified in the results section, mice were gavage an equivalent of one kilocalorie of the indicated substance (Abbott Promote) twice a day to provide nutrition and maintain euglycemia.

For the antiviral response experiments, eight-week-old AMPKα1/$\alpha2^{Flox}$+Lyz^{Cre-} and AMPKα1/$\alpha2^{Flox}$+Lyz^{Cre+} mice were tail intravenously injected with gVSV by a dose of $1x10^7$ pfu per gram of animal weight. Mice were sacrificed at 12 hpi, and the PBMCs were isolated from the animal blood using Percoll (Sigma). The mRNA level of VSV and the expression of ISGs were analyzed and quantified by qRT-PCR to determine the influence of AMPK on the antiviral responses.

For virus infection and blood glucose level measurement, mice were starved for 2 hours, and a drop of blood was collected by snipping the very end of the tail and analyzed in a VivaChek Ino strip, which was counted using the VivaChek Ino glucometer to measure the blood glucose levels. Mice were injected intravenously with viruses gVSV and HSV-1, or with the gavage of viruses MRV and SADS-CoV. The glucose levels in murine blood were measured at the indicated time by the VivaChek Ino glucometer.

Murine Corneal HSV-1 Infection

The BALB/c or CL57B/6 mice at four- to six-week-old were infected on the right eyes with 1×10^6 pfu of HSV-1 and left eyes with DMEM without epithelial debridement. At 1 dpi, PBS containing DMSO (mock) or AICAR (2 mM) was topically applied to both eyes once a day. Two observers performed ocular disease scoring (0-5, 5 being severe) in a blinded fashion based on the following scoring system: 0-no symptoms, 1-mild symptoms with < 20% eyelid shut, 2-moderate symptoms with 20 - 50% shut, 3-moderate symptoms with 50 - 80% shut, 4-severe symptoms with > 80% shut, 5-eye completely shut with crusting. Mice were sacrificed at 6 dpi, and the eyeballs or eyelids were collected for quantitative RT-PCR assay by using the HSV-1 primer

Please cite this article in press as: Zhang et al., AMPK directly phosphorylates TBK1 to integrate glucose sensing into innate immunity, Molecular Cell (2022), https://doi.org/10.1016/j.molcel.2022.10.026

sequences (5'-GGCCTGGCTATCCGGAGA-3', 5'-GCGCAGAGACATCGCGA-3'). Mice were maintained under specific pathogen-free (SPF) conditions.

Nano-liquid Chromatography/Tandem MS (Nano LC-MS/MS) Analysis

Nano LC/tandem MS analysis for protein identification and characterization and label-free quantification was performed by Phoenix National Proteomics Core services. Briefly, tryptic peptides were separated on a C18 column and analyzed by LTQ-Orbitrap Velos (Thermo). Proteins were identified using the National Center for Biotechnology Information search engine against the human or mouse RefSeq protein databases. The mass spectrometry proteomics data of TBK1 modifications by AMPK have been deposited to the ProteomeXchange Consortium (http://proteomecentral.proteomexchange.org) via the iProX partner repository with the dataset identifier PXD033926.

CE-MS-based Measurement of AMP, ADP, and ATP

The sample preparation for CE (capillary electrophoresis)-MS was carried out as described previously.[90] Briefly, cells at 70–80% confluence and with specified treatments were rinsed with 5% mannitol solution and instantly frozen in liquid nitrogen, lysed with methanol containing the internal standards 1 (IS1, Human Metabolome Technologies, H3304-1002, 1:200), which was used to standardize the metabolite intensity and adjust the migration time. The lysates were mixed with the buffer of chloroform and water, vortexed by 20 s, and centrifuged at 15,000 g for 15 min at 4 °C. A 450 μL of the aqueous phase was collected and ultrafiltrated through an Ultrafree-MC-PLHCC centrifugal filter at 10,000 g for 3 h at 4 °C. The ultrafiltrated products were then freeze-dried and dissolved in 100 μL of ultrapure water containing IS2 (1:200), and a 20 μL of the re-dissolved solution was loaded into an injection vial with a conical insert for analysis by CE-TOF MS (Agilent Technologies 7100, equipped with 6224 mass spectrometers).

GC-MS-based Measurement of Long-Chain Fatty Acids (LCFAs)

Some 100 μL of mouse serum was instantly mixed with 1 mL of methanol containing 40 μg/mL tridecanoic acid as an internal standard, followed by 20 s of vortexing. After centrifugation at 15,000 g for 15 min at 4°C, 400 μL of supernatant (aqueous phase) was freeze-dried at 4°C. The lyophilized sample was then vortexed for 1 min after mixing with 1 mL of freshly prepared 1% H_2SO_4 (v/v in methanol), then incubating at 80°C for 1 h. The esterified products were then extracted by vigorously mixing with 2 mL of hexane three times at room temperature. The organic (upper) phase was collected and then dried in the nitrogen flow at room temperature. Before subjecting to GC-MS, the sample was dissolved in 1 ml of hexane, followed by centrifuging at 15,000 g for 10 min, and some 60 μL of supernatant was loaded into an injection vial. GC (gas chromatography) was performed on a CP-Wax 52 CB column (30 m × 0.25 mm i.d., 0.25 μm film thickness) using a 7890B Agilent (Agilent Technologies) instrument fitted with an MS detector (5977B Agilent). The injector temperature was 260°C. The column oven temperature was initially held at 50°C for 3 min and next increased firstly to 170°C at the rate of 10°C/min and then to 205°C at the rate of 3°C/min, where it was held for 20 min, subsequently to 235°C at the rate of 5°C/min and finally to 250°C at the rate of 10°C/min, where it was held for 3 min. The MSD transfer temperature was 280°C. The MS quadrupole and source temperature were maintained at 150 and 230°C, respectively. GC mass data were analyzed using MassHunter software from Agilent Corp.

QUANTIFICATION AND STATISTICAL ANALYSIS

Quantitative data are presented as the mean ± standard error of the mean (SEM) from at least three independent experiments. When appropriate, the statistically significant differences between multiple comparisons were analyzed using the one-way or two-way ANOVA test with Bonferroni correction. Differences were considered significant at $p<0.05$. All samples were included in the analyses if preserved and properly processed, and no samples or animals were excluded except for zebrafish with conventional injection damage. No statistical method was used to predetermine sample size, and all experiments except those involving animals were not randomized. Immunoblotting, reporter assays, and qRT-PCR experiments have been repeated a minimum of three times independently to ensure reproducibility. The investigators were not blinded to allocation during experiments and outcome assessment.